8-2021

EXPERIMENTAL ALTERATION OF VENUSIAN SURFACE BASALTS IN A HYBRID CO2-SO2 ATMOSPHERE

Robert B. Reid
University of Tennessee, Knoxville, rreid8@vols.utk.edu

To the Graduate Council:

I am submitting herewith a thesis written by Robert B. Reid entitled "EXPERIMENTAL ALTERATION OF VENUSIAN SURFACE BASALTS IN A HYBRID CO2-SO2 ATMOSPHERE." I have examined the final electronic copy of this thesis for form and content and recommend that it be accepted in partial fulfillment of the requirements for the degree of Master of Science, with a major in Geology.

Molly C. McCanta, Major Professor

We have read this thesis and recommend its acceptance:

Annette S. Engel, Nicholas J. Dygert

Accepted for the Council:
Dixie L. Thompson

Vice Provost and Dean of the Graduate School

(Original signatures are on file with official student records.)

EXPERIMENTAL ALTERATION OF VENUSIAN SURFACE BASALTS IN A HYBRID CO_2-SO_2 ATMOSPHERE

A Thesis Presented for the
Master of Science
Degree
The University of Tennessee, Knoxville

Robert B. Reid
August 2021

Abstract

Venus' surface and interior dynamics remain largely unconstrained, due in great part to the major obstacles to exploration imposed by its 470°C, 90 bar surface conditions and its thick, opaque atmosphere. Orbiter-based thermal emission data provide an opportunity to characterize the Venus surface. However, interpretations of such spectra critically depend on understanding interactions between the planet's surface basaltic rocks and its caustic, sulfur dioxide (SO_2)-bearing carbon dioxide (CO_2) atmosphere. Several studies, using remote sensing, thermodynamic modeling, and laboratory experiments, have placed constraints on basaltic alteration mineralogies and rates. Yet constraint with respect to SO_2-mediated reactions with basalts of contrasting compositions remains incomplete. Here, we present new data from a series of gas-solid reaction experiments, in which samples of two basalt compositions were reacted in an SO_2-bearing CO_2 atmosphere, at relevant Venus temperatures, pressure, and oxygen fugacity. We subjected reacted specimens to scanning electron microscopy analyses where their surface alteration products were characterized and their abundances estimated. We demonstrate that metathenardite and anhydrite are the prevalent alteration products on alkaline and tholeiitic basalt samples, respectively, and Fe-oxide phases are minor. Moreover, alteration products may completely cover alkali samples within a few weeks and tholeiite specimens within ~60 years. We suggest that these rates indicate that some unweathered volcanic features observed on Venus, as determined from emissivity intensity contrasts, may have been emplaced within a few weeks to less than 100 years before they were detected.

Table of Contents

Section 1. Introduction 1
Current Constraints of Reaction Mechanisms and Rates on the Venus Surface 2
Section 2. Background 4
Venus' Surface Properties 4
Thermodynamic Models of Basalt Alteration on Venus' Surface 5
Experimental Constraints of Basalt Alteration on Venus' Surface 5
Constraints on Basalt Alteration Using Thermal Emissivity 8
Section 3. Starting Materials and Methods 9
Starting Materials 9
Experimental Setup 9
Analytical Methods 10
Surface characterization using SEM (BSE and EDS) 10
Cross section sample preparation (FIB) 10
Section 4. Results 12
Surface Alteration in the Presence of SO_2 Gas 12
Alkaline Basalts 12
Tholeiitic Basalts 13
Surface Alteration in a Pure CO_2 Atmosphere at 90 Bars, MH fO_2 13
Alkaline basalts 13
Tholeiitic basalts 14
Section 5. Discussion 15
SO_2-Bearing Experiments 15
Effect of Starting Composition on Reaction Products and Coverage 15
Effect of Run Duration on Reaction Products and Coverage at 470°C, 90 Bars, and Magnetite-Hematite fO_2 17
Effect of Varying Run Temperature on Reaction Products and Coverage 18
Comparison between CO_2-only and CO_2+SO_2 experimental atmospheres 18
Alteration Rates and Venus' Surface Age Constraints 19
Section 6. Summary 22
Section 7. Future Work 24
List of References 25

Appendix. Tables and Figures 32
Vita..... 45

List of Tables

Table 1. Venera and Vega geochemical analyses of Venus' surface rock compositions..... 32
Table 2. Chemically active major and trace gases in Venus' atmosphere..... 32
Table 3. EPMA analyses of starting materials (Teffeteller et al., 2020, 2021a, 2021b. 33
Table 4. Experimental runs with sample compositions, conditions, and durations. 33
Table 5. Alteration product coverage of reacted alkali and tholeiite samples. 34

List of Figures

Figure 1. Log oxygen fugacity (fO_2) of several mineral redox buffers plotted as a function of temperature at 1 bar pressure 34
Figure 2. VIRTIS emissivity data with superimposed Magellan SAR map of the volcano Idunn Mons (L) and emissivity in Venus' southern hemisphere (R) 35
Figure 3. Schematic of a generic cold-seal pressure vessel apparatus. 36
Figure 4. A representative transect superimposed on a SEM microphotograph of the surface of a basalt sample. 36
Figure 5. SEM z-contrast photomicrograph of a FIB milling protective carbon cap 37
Figure 6. SEM secondary electron microphotograph of the surface of a sample after gallium ion milling of two opposing trenches that defined the FIB cross-section. 37
Figure 7. SEM z-contrast microphotograph of completed FIB cross-section from specimen VS-1A. 38
Figure 8. Graphic depicting alteration product relative abundances on alkali (A) and tholeiite (B) specimens. 39
Figure 9. SEM BSE images of alkali samples. 40
Figure 10. SEM BSE images of tholeiite samples 41
Figure 11. Graphic showing estimated abundances of alteration phases on run products reacted in pure CO_2 42
Figure 12. SEM BSE microphotographs of samples reacted for two weeks in pure CO_2 at 90 bars 43
Figure 13. Schematic depicting basalt glass reactions in gases at 470°C, 90 bars pressure for 2 weeks at MH fO_2 44

Section 1. Introduction

Venus' volcanic shield edifices, volcanic plains, and lava flow morphologies, as well as its caustic atmosphere, are the products of abundant volcanism (Head et al., 1992; Nimmo & McKenzie, 1998; Basilevsky et al., 2007; Taylor & Grinspoon, 2009; Marcq et al., 2012). Impact crater statistics suggest that volcanism resurfaced approximately 80% of the planet in basaltic material ~600–300 Ma (Nimmo & McKenzie, 1998). In-situ constraints on the surface basalt compositions, shown in Table 1 (All Tables and Figures may be found in the Appendix), have been limited to just three individual analyses collected from its lava plains and rises by the Soviet Venera 13–14 (1981) and Vega 2 (1984) lander missions (Barsukov et al., 1982; Surkov & Barsukov, 1985). Though the data contain large uncertainties, the elemental chemistries are consistent with the compositions of terrestrial tholeiite and alkali basalt endmembers (Barsukov et al., 1982; Surkov & Barsukov, 1985; Treiman, 2007; Filiberto, 2014).

At ~470°C and 90 bars pressure, Venus' surface basalts interact with an oxidizing atmosphere that has an oxygen fugacity (fO_2) near the magnetite-hematite (MH) buffer (Fig 1; Pieters et al., 1986; Fegley et al., 1995; Fegley et al., 1997; Fig. 1) The atmosphere is composed of approximately 96.5% carbon dioxide (CO_2) and 3.5% nitrogen (N_2), with minor abundances of H_2O (water) and other trace gases (Table 2; Barsukov et al., 1982; Seif et al., 1985; Bézard & de Bergh, 2007). The highly reactive gas, sulfur dioxide (SO_2), is ~10^6 times greater in abundance (~150 ppmv, parts-per-million by volume) than that in Earth's atmosphere and interacts with Venus' surface (Marcq et al., 2012). In this hot and caustic atmosphere, Venus' basaltic rocks have likely been extensively altered over the ensuing several hundred million years.

Unlike Mars, Mercury, and the Moon, Venus' atmosphere precludes detailed spectroscopic studies of its surface (Esposito, 1984; Moroz, 2002). However, there are several atmospheric emissivity windows near 1 um that can be used to gather spectral data that constrain surface composition (Carlson et al., 1991; Moroz, 2002; Hashimoto & Sugita, 2003; Mueller et al., 2008). Variations in surface emissivity intensity (Fig. 2) have been interpreted as evidence of magnetite (Fe_3O_4) and/or hematite (Fe_2O_3) alteration products coating Venus' rocks (Pieters et al., 1986; Smrekar et al., 2010; Kappel et al., 2016). Anomalous emissivity highs have been detected in regions around some of Venus' volcanic centers and their associated lava flows (e.g., left image, Fig. 2). These excursions have been hypothesized to be unweathered basalt produced during volcanic episodes occurring within the last 2.5 million to 250,000 years (Smrekar et al., 2010; Stofan et al., 2016; D'Incecco et al., 2017; Mueller et al., 2020). However, exponential atmospheric SO_2 fluctuations observed by NASA's Pioneer Venus orbiter in the 1980s and ESA's Venus Express orbiter in the 2000's could have resulted from present day volcanic activity (Esposito, 1984; Nimmo & McKenzie, 1998; Glaze, 1999; Marcq et al., 2012). Recent basalt oxidation studies have supported this interpretation, suggesting it is possible that volcanism is currently active on Venus (Cutler et al., 2020; Filiberto et al., 2020; Teffeteller et al, 2020, 2021a, b). Confirmation of recent volcanism on Venus' surface would herald a shift in our

understanding of the planet's mantle state and thermal history paradigms, particularly in the last ~1000 Myr.

Current Constraints of Reaction Mechanisms and Rates on the Venus Surface

Chemical alteration on Earth's surface occurs in the presence of water. Though Venus' deep atmosphere is dry in comparison (~30 ppm H_2O; Table 2), thermodynamic work suggests that atmospheric interaction with the planet's surface rocks is chemically favorable, yielding secondary mineral coatings of magnetite ± hematite and anhydrite ($CaSO_4$) (Barsukov et al., 1982; Surkov & Barsukov, 1985; Pieters et al., 1986; Fegley & Treiman, 1992; Treiman, 2007; Zolotov, 2018). Determining the rate at which these coatings are accumulating may help constrain the ages of Venus' surface features (e.g., Fegley & Prinn, 1989). However, as it is unlikely that Venus' trace water participates in basalt alteration (Surkov & Barsukov,1985), it has been proposed that this alteration rate is significantly slower than that on Earth (Fegley & Treiman, 1992).

Foundational experimental work (Cook et al., 1990; Cooper et al., 1996) has established that high temperature basalt alteration in sulfur-free atmospheres occurs via oxidation that is accompanied by the diffusive migration of Fe^{2+} (ferrous iron), Mg^{2+} (magnesium), Ca^{2+} (calcium) and Na^{1+} (sodium) from the interior to the free surface of the basaltic material, forming oxide phases at the solid-gas interface. Cation migration generates a gradually thickened alteration layer in the subsurface of the sample body. Cook et al. (1990) propose that the rate of alteration proceeds in inverse proportion to the square root of time ($Zm^2 = 2 * k' * t$, where t is duration, Z_m is the thickness of layer 'm', and k' is the parabolic rate constant [e.g., Crank, 1980; Cook et al., 1990]). Using this rate principle, further experimental alteration work using basalt-analog materials and sulfur-free atmospheres has led to estimates that Venus volcanic activity may have been occurring no more than a few hundred thousand to a few hundred years before detection (Teffeteller et al, 2020, 2021a, b). Studies using an implied linear alteration rate estimate that this volcanic activity may have occurred as recently as a few years to months before it was detected (Cutler et al., 2020; Filiberto et al., 2020). These more recent sulfur-free experiments yielded alteration rates based on reactions at 470–900°C between mafic minerals or basalts and pure CO_2 or terrestrial air atmospheres, that produced surface coatings of iron oxides as reaction products. Yet, only samples from Teffeteller et al. (2020, 2021a, b) were reacted at Venus' surface temperature of 470°C. The 600–900°C temperature and ambient water conditions in both Filiberto et al. (2020) and Cutler et al. (2020), and the absence of SO_2 in the reactant gases in all of the aforementioned studies make uncertain how applicable their reaction rates and products are to Venus' surface.

Several alteration experiments, using analogous basaltic materials reacted in SO_2-bearing atmospheres, showed that the highly reactive SO_2 gas readily alters basaltic rocks, likely via covalent chemisorption reactions (Henley et al., 2015; King et al., 2018; Palm et al., 2018; Renggli & King, 2018; Berger et al., 2019; Renggli et al., 2018, 2019). Surficial reaction phases produced in the experiments, primarily anhydrite, magnetite ± hematite, and to a lesser extent, metathenardite (Na_2SO_4) and glauberite [$Na_2Ca(SO_4)_2$], are similar to those documented on

Hawaiian basalts that were altered by SO_2-rich gases at an active volcanic vent (McCanta et al., 2014). Moreover, the experimental alteration rate involving SO_2 gas was reported to be hundreds of nanometers to several microns per week, and produced mainly Ca-sulfates and minor Na-sulfate and Fe-oxide secondary minerals based on bulk rock composition and experimental temperatures (Henley et al., 2015; King et al., 2018; Palm et al., 2018; Renggli & King, 2018; Berger et al., 2019; Renggli et al., 2018, 2019). Only the experiments from Berger et al. (2019) were conducted with an atmospheric SO_2 concentration (150 ppm) and temperature (475°C) analogous to Venus' surface. Oxygen fugacity was buffered at the nickel-nickel oxide (NNO) buffer, which is significantly less oxidizing than the fO_2 (MH buffer; Fig. 1) estimated for Venus' surface. Other studies used pure SO_2 gas and temperatures ≥600°C in their experiments, which are atmospheres and temperatures unlike those found on Venus (Henley et al., 2015; King et al., 2018; Palm et al., 2018; Renggli & King, 2018; Renggli et al., 2018, 2019). Therefore, it remains unclear if these SO_2-bearing studies have produced reactions that accurately reflect those on the surface of Venus.

To date, constraints on the mineralogy of Venus' primary surface rocks, their alteration products, and the rates at which alteration occur remain incomplete. As the compositions of surface igneous rocks are the sole means available to interpret Venus' interior state, additional experimental work that addresses these parameters is needed to aid in interpreting both past and future remote sensing data accurately and would thereby unlock crucial data points to deducing Venus' geodynamic evolution. Thermodynamic models are theoretical and do not provide a complete understanding of likely reaction products and rates for conditions so far outside their calibration inputs. Laboratory experiments broadly define these uncertainties but have yet to consider the combined effects of Venus' CO_2+SO_2 atmosphere and Venus surface temperature, pressure, and oxygen fugacity.

This study addresses these ambiguities, experimentally, by isolating the effect of SO_2 on gas-solid reactions with materials, atmospheres, and conditions that simulate those at Venus' surface. New data are presented that were collected from a series of gas-solid reaction experiments, in which samples of two basalt compositions were reacted in an SO_2-bearing CO_2 atmosphere, at relevant Venus temperature, pressure, and fO_2, and compared with data from previous work. The hypotheses investigated are: **1)** the alteration products occurring on Venus' rocks are dominated by Ca- and Na-sulfates with minor magnetite/hematite; **2)** bulk composition is the primary control on secondary mineralogy; and **3)** reaction rates are likewise dependent on bulk chemistry. The results of these experiments place constraints on alteration products, thicknesses, and effects on emissivity. These data are then used to calculate surficial age limits based on previously collected emissivity data and to provide new means of interpreting geochemical data returned by future missions.

Section 2. Background

Venus' Surface Properties

Although Venus is similar in size, mass, and bulk chemistry to Earth, its atmospheric composition and surface conditions are quite different. Venus' departure from a common evolutionary arc with Earth, sometime before it was catastrophically resurfaced approximately 300–600 Ma (Nimmo & McKenzie, 1998; Taylor & Grinspoon, 2009; Kane et al., 2019), has produced an opaque atmosphere that thwarts observation of the surface over most of the electromagnetic spectrum. Subsequent greenhouse heating has resulted in an estimated surface temperature of 470°C and pressure of ~92 bars (Seif et al., 1985) that have neutralized lander electronics within minutes of touchdown. As a result, in-situ major element geochemical data are limited to just three observations from Venus' surface in the form of X-ray fluorescence (XRF) analyses, presented in Table 2, that were collected in Venera 13–14 and Vega 2 lander missions (Surkov & Barsukov, 1985). Although the analyses contained large uncertainties, and mineralogy was not constrained, it was suggested that the two primary basalt compositions were analogous to a terrestrial alkaline plume basalt and a tholeiitic mid-ocean ridge basalt, each having chemically interacted with Venus' sulfur-bearing atmosphere (Barsukov et al., 1982; Surkov & Barsukov, 1985; Treiman, 2007; Filiberto, 2014). However, Surkov & Barsukov (1985) propose that the reactions had not gone to completion, and that the low abundance of atmospheric water (Table 2) precluded the involvement of H_2O.

Two independent lines of evidence suggest that the oxygen fugacity (fO_2) of Venus' near-surface atmosphere is approximately at the magnetite-hematite (MH) buffer, at lower elevations: **1)** multispectral images and reflectance spectra of Venus' surface that were collected in Venera 9, 10, and 13 lander missions indicate that the planet's rocks are coated with magnetite and hematite that likely buffer the near-surface fO_2 (Pieters et al., 1986); and **2)** thermodynamic modeling by Fegley et al. (1995, 1997) with respect to the Venera/Vega rock chemistries and Venus' atmospheric carbon dioxide (CO_2) and carbon monoxide (CO) ratios indicate that both magnetite and hematite are stable products of oxidation. Models assume that Venus basalts formed at the more reduced quartz-fayalite-magnetite (QFM) buffer, a similar fO_2 to that of terrestrial basalts. Therefore, the oxidation potential gradient between QFM and MH oxygen fugacity buffers that would drive the reactions is consistent with the production of magnetite and hematite observed on Venus' surface (Fegley et al., 1995, 1997). At the MH fO_2 buffer, atmospheric sulfur is oxidized, as well, and most likely speciates as sulfur dioxide (SO_2), which reacts with calcium (Ca) and sodium (Na) in Venus' rocks to form secondary sulfate products (Surkov & Barsukov, 1985; Fegley & Treiman, 1992).

Thermodynamic Models of Basalt Alteration on Venus' Surface

Several thermodynamic studies have proposed that reactions, via simultaneous oxidation and sulfatization, occur between Venus' rocks and its CO_2-rich, SO_2-bearing atmosphere, and produce stable secondary products of Fe-oxides and Ca-sulfates. Calculations having Na-sulfate and carbonate products are not included as they were suggested to be unstable on Venus' surface (Zolotov, 2018 and references therein). With respect to the aforementioned constraints on kinetics, reactants, and fO_2, the predicted reactions are outlined in the following equations, beginning with oxidation (e.g., Fegley et al.,1997; Zolotov, 2018):

$$3FeO \text{ (in silicates)} + CO_{2(g)} \rightarrow Fe_3O_4 \text{ (magnetite)} + CO_{(g)}; \quad (1)$$

which may further partially oxidize via (Fegley et al., 1997):

$$2Fe_3O_4 \text{ (magnetite)} + CO_{2(g)} \rightarrow 3Fe_2O_3 \text{(hematite)} + CO_{(g)}; \quad (2)$$

and by sulfatization (e.g., Treiman, 2007; Zolotov et al., 2018):

$$CaO \text{ (in minerals and glasses)} + 1.5SO_{2(g)} \rightarrow CaSO_4 \text{(anhydrite)} + 0.25S_{2(g)}. \quad (3)$$

Igneous silicate phases in exposed rocks would produce residual phases of Si, Mg, Al, and Na, as well as sulfates, such as (Zolotov, 2018):

$$CaMgSi_2O_6 \text{(diopside)} + 1.5\ SO_{2(g)} \rightarrow CaSO_4 + MgSiO_3 \text{(enstatite)} + SiO_2 + 0.25S_{2(g)}; \quad (4)$$

and

$$CaAl_2Si_2O_8 \text{(anorthite)} + 1.5\ SO_{2(g)} \rightarrow CaSO_4 + Al_2SiO_5 \text{(andalusite)} + SiO_2 + 0.25S_{2(g)}. \quad (5)$$

Software-based thermodynamic models in Simprech et al. (2020) corroborate the products and reactions in the above equations, which allow for the additional stability of cordierite ($Mg_2Al_4Si_5O_{18}$). Results did not include reactions that produce Na-sulfate phases due to their absence from the databases that were used in their models. To that end, thermodynamic models are limited by their inputs and merely provide an approximation for possible reactions and, therefore, underscore the need for experimentation to further constrain reaction kinetics, products, and rates, notably with consideration for Na-rich basaltic rocks, where Na reacts with SO_2 to form metathenardite via:

$$Na_2O \text{ (in minerals and glasses)} + 1.5SO_{2(g)} \rightarrow Na_2SO_4 \text{(metathenardite)} + 0.25S_{2(g)}. \quad (6)$$

Experimental Constraints of Basalt Alteration on Venus' Surface

High temperature (550–800°C) oxidation experiments of basalt analog glasses reacted in air at atmospheric pressure reveal that network modifying cations, Fe^{2+}, Mg^{2+}, and Ca^{2+} diffusively migrate toward the free surface from the interior of the glass (Cook et al. 1990; Cooper et al., 1996). Therefore, it was suggested that diffusive cation migration is induced by the oxidation potential created by the contrasting oxidizing fO_2 of Earth air (~10 log units above quartz-fayalite-magnetite [QFM] buffer; McCammon, 2005) versus that of basaltic glass equilibrated at a more reduced fO_2, near the quartz-iron-fayalite (QIF) buffer (Fig. 1). It was also shown that Mg^{2+} and Ca^{2+} form oxides (MgO and CaO) at the surface, and Fe^{2+} oxidizes to Fe^{3+} producing surficial magnetite (Fe_3O_4) and hematite (Fe_2O_3). Subsurface Fe^{2+} is also oxidized to Fe^{3+}, thus becoming a network former in the silicate substrate. Na^{1+} migrates in the subsurface to charge-balance both oxidizing Fe and vacancies created by the migrating divalent cations, charge-compensating by the inward flux of electron holes. Moreover, it was proposed that diffusive migration of divalent cations is the rate-limiting factor in basalt glass oxidation and that alteration depth is inversely proportional to the square root of duration, which established a potential basalt alteration chronometer (Cook et al. 1990; Cooper et al., 1996). The composition and fO_2 of terrestrial air and the study's temperature and pressure conditions were not analogous to Venus' surface. Therefore, it was uncertain how applicable their results were to reactions on Venus.

Filiberto et al. (2019) show that olivine grains, major constituents of some basalts, that were oxidized in air at 600 and 900°C at 1 bar, exhibit Fe-oxide coatings that progress over their surfaces over a 26-day duration. Using the same conditions, Cutler et al. (2020) observe similar reactions on basaltic materials spanning a 7-week experimental period. In both studies, reflectance spectra were taken of the resultant secondary mineral coatings in the near-infrared (NIR;1000 nm wavelength). Spectra changed from that characteristic of the primary materials, to that consistent with magnetite, and later, hematite. It was proposed that secondary Fe-oxide mineralization can rapidly obscure the VNIR emissivity signal (suggested to be analogous to 1 minus reflectance) on the surfaces of olivine grains and glassy basalts. Therefore, "fresh" lava flows at Idunn Mons (Fig. 2), previously estimated to be 250,000–2.5 m.y. old (Smrekar et al., 2010), were suggested to have been emplaced within a few months to a few years before they were detected.

Similar results to Filiberto et al. (2019) and Cutler et al. (2020) are reported by Teffeteller et. al (2020, 2021a, b) in a series of oxidation experiments using glassy alkaline and tholeiitic basalt materials. Reactions were conducted at more Venus-relevant conditions—470 and 700°C, in a pure CO_2 atmosphere, at 90 bars pressure, and buffered at MH fO_2. As discussed by Cook et al. (1990) and Cooper et al. (1996), zones of cation enrichment bounded by zones of depletion in the subsurface were observed on their run products, which were interpreted as evidence of diffusive migration of divalent cations from the interior of the glass to the surface. Cation migration was the rate-limiting factor of alteration. A discontinuous coating of Fe-oxide alteration products was observed on sample surfaces. Siderite ($FeCO_3$) and minor calcite

($CaCO_3$) secondary phases were also noted. Using alteration zone thicknesses and reaction durations, a slower alteration rate than that implied by Filiberto et al. (2019) and Cutler et al. (2020) was calculated to suggest that volcanic activity could have occurred 3,000–11,000 years ago. However, none of these works considered Venus' atmospheric SO_2 in their experiments.

SO_2-rich gas readily alters basalt in terrestrial settings (i.e., H_2O- and O_2-bearing air) and produces coatings of sulfate minerals on rock surfaces (McCanta et al., 2014). As alteration proceeds in this setting, an amorphous silica layer forms beneath the surface, which may serve as barrier to further interaction with atmospheric gases, and thereby halt activity on the surface. However, it is unlikely that Venus' ~30 ppmv H_2O participates in surface reactions at such extreme temperatures (Surkov & Barsukov, 1985). Henley et al. (2015) experimentally explore the sulfate forming mechanism in gas-solid reactions, using a range of temperatures, 600–800°C, between plagioclase endmembers and pure SO_2 gas. They conclude that, instead of disproportionation in the formation of sulfate ions—a common reaction in aqueous environments—the reactions at temperatures >400°C are governed by a chemisorption process, where SO_2 covalently bonds directly to the surface of the solid and reacts vigorously with Ca (and Na) cations to form sulfates at the gas-solid interface. Minor Fe-oxides can develop on the surface, as well, in response to the oxidizing SO_2 gas. A subsequent suite of investigations was conducted at similar conditions, reacting pure SO_2 with natural basalts and basalt-analog glasses over the range of 10 minute to 24-hour durations (King et al., 2018; Palm et al., 2018; Renggli & King, 2018; Renggli et al., 2018, 2019). Despite the absence of water in the experiments, sulfate and Fe-oxide alteration phases were produced on all samples, supporting the chemisorption hypothesis, and suggesting a similar process could be governing reactions on Venusian rocks. Moreover, cross sections of samples exhibited chemical layering of cations that corroborated a migrating cation mechanism of alteration that was likely the alteration rate-limiting factor. As experiments were conducted in pure SO_2 at 1 bar pressure, it was unclear what effect(s) pressure and trace amounts of SO_2 have on temperature-mediated chemisorption reactions on Venus.

Experiments that address these uncertainties were conducted by Berger et al. (2019) through a series of high temperature, high pressure investigations that tested the reactions between a variety of basaltic materials and atmospheres. Among them were runs performed at 475°C, 90 bars pressure that reacted tholeiitic basalt, vitreous synthetic alkali basalt, and pumice in a Venus-like atmosphere with 96% CO_2, 3% N_2, and 150 ppm SO_2, near the nickel-nickel oxide (NNO) fO_2 buffer. Results showed that abundant sulfate phases—anhydrite ($CaSO_4$), metathenardite (Na_2SO_4), and glauberite [$Na_2Ca(SO_4)_2$]—crystallized on the samples' glassy surface, and olivine grains were coated with Fe-oxides in the crystalline basalts. The distribution of Na, Ca, and Mg cations suggested that they had migrated towards the surface, leaving a cation-depleted zone beneath the surface that was also associated with secondary crystallization of dendritic magnesioferrite ($Mg(Fe^{3+})_2O_4$). The oxidation of iron to produce magnesioferrite and the migration of network-modifying cations were consistent with results from prior studies (Cook et al., 1990; Cooper et al., 1996). But the mechanism for producing anhydrite, for example, was less clear. Sulfatization via the chemisorption of SO_2, as proposed by Henley et al. (2015), could not be observed. Therefore, it was suggested that CaO, resulting from oxidation of Ca at the surface, was converted to anhydrite upon reaction with SO_2, in a mechanism consistent

with that offered by Cooper et al. (1996). Laboratory experiments, which have been crucial to constraining microscale weathering phenomena that may occur on Venus, have provided data that may be used to constrain the surface expressions of gas-solid reactions occurring globally, as observed by orbiting spacecraft.

Constraints on Basalt Alteration Using Thermal Emissivity

Venus' extreme temperature and opaque atmosphere have posed major obstacles to examining its surface to constrain primary and secondary surface rock compositions. Nevertheless, it has been established that: **1)** Venus' atmosphere is relatively transparent in electromagnetic spectral windows near 1μm (Carlson et al., 1991; Moroz, 2002; Hashimoto & Sugita, 2003; Mueller et al., 2008) that permit the surface to be resolved from orbit in terms of thermal emissivity; **2)** the surfaces of Venus' Fe^{2+}-bearing basalts have oxidized, producing coatings of magnetite and hematite weathering products (Pieters et al., 1986; Fegley et al., 1995, 1997); and **3)** intensity contrasts in thermal emissivity can be used to discern hematite and magnetite from unweathered ferromagnesian silicates, where elevated emissivities correlate directly with richer Fe^{2+} contents (Pieters, 1983; Carlson et al., 1991). The synthesis of these principles was used to evaluate the surface in Venus' southern hemisphere using the visible and infrared thermal imaging spectrometer (VIRTIS) instrument on the European Space Agency's Venus Express orbiter.

Data, shown in Figure 2, collected from VIRTIS reveal regions with anomalously high emissivity around several of the planet's volcanic plume and coronae morphologies, which have been interpreted as evidence that their rocks have experienced little interaction with the atmosphere. Hence, they appear fresh and are suggested to have been emplaced in geologically recent volcanic events (Smrekar et al., 2010; Gilmore et al., 2015; Smrekar et al., 2014; Stofan et al., 2016; D'Incecco et al., 2017; Mueller et al., 2017). This hypothesis is consistent with observations made from radar emissivity (Brossier et al. 2020), stratigraphic correlation of lava flows (D'Incecco et al., 2017; Mueller et al., 2017), as well as the contrasting anomalously low emissivities of stratigraphically old tesserae morphologies (Gilmore et al., 2015, 2017). Subsequent work has proposed that VIRTIS emissivity contrasts may even be used to infer total FeO content (wt %) of Venus' surface rocks, that may aid in distinguishing primary mafic/ultramafic versus more evolved rock compositions (Helbert et al., 2021).

In sum, previous studies demonstrate that Venus' surface exhibits variable emissivity intensities that indicate a range of degrees of alteration and/or different primary rock compositions. These interpretations largely exclude sulfate alteration products that are likely to occur. Dyar et al. (2020) suggest that sulfates, not hematite, may be the dominant alteration mineralogy on Venus' rocks, and emission spectra reflect sulfate coatings of variable thicknesses. Yet, constraint of the mineralogy and surface coverage rates of precipitating sulfates is lacking. Moreover, few data exist with respect to their effects on emissivity spectra (Dyar et al. 2020).

Section 3. Starting Materials and Methods

Starting Materials

The mafic glass samples for these experiments are chemically similar to the rocks analyzed on Venus' surface and were chosen to allow for testing the effects of contrasting bulk composition and vitreous versus phenocrystic materials on reaction rates and alteration mineralogy. Two starting compositions were used: a natural alkaline basalt (composition A) containing crystalline phases, from Sverrefjell volcano, Svalbard, Norway (Skjelkvåle et al., 1989), compositionally similar to the Venera 13 volcano plume basalt (Table 1; Barsukov et al., 1982; Surkov & Barsukov, 1985; Barsukov et al., 1986; Treiman, 2007); and a tholeiite glass (composition B), analogous to Venus' plains basalts (Barsukov et al., 1982; Surkov & Barsukov, 1985; Barsukov et al., 1982; Treiman, 2007), synthesized using the XRF data collected from the Venera 14 and VEGA 2 missions (Filiberto, 2014). Due to the large uncertainty of the Venera 13, 14 and VEGA 2 bulk analyses, as well as sodium not being measured by any lander, adjustments were made to ambiguous element abundances to produce the synthetic glass based on experimental and thermodynamic studies of basaltic melts (Table 3; Surkov & Barsukov, 1985; Treiman, 2007; Filiberto, 2014).

Prior to experimentation, alkali samples were cut and polished into 1 mm-thick chips and characterized using the Cameca SX-100 electron probe micro-analyzer (EPMA) at the University of Tennessee, Knoxville. Modal abundances and average mineral and glass compositions were subsequently used to calculate bulk composition (Table 3; Teffeteller, 2020, 2021a, b). The tholeiitic glass was prepared using reagent grade oxides and homogenized and fused at 1300°C, 1 atm, and the quartz-magnetite-fayalite (QFM) fO_2 buffer. The melt was rapid-quenched and broken into fragments suitable for inclusion in cold-seal pressure vessels. The tholeiitic composition was also verified using EPMA (Table 3; Teffeteller, 2020, 2021a, b).

Experimental Setup

Three experiments (VS-1, VS-3, and VS-4) were run in cold-seal pressure vessels, similar to that depicted in Figure 3, in the laboratory of Mac Rutherford at Brown University. Experimental conditions for samples VS-1 (A and B) were 700°C, 90 bars and a 14-day duration. The durations of the two remaining experimental runs, conducted at Venus' surface conditions, 470°C, 90 bars, were as follows: VS-3 (A and B), 22 days, and VS-4 (A and B), 30 days (Table 4). The 470°C temperature was selected to approximate Venus' surface temperature at low elevations and to isolate the effect of time, while the 700°C temperature was chosen to increase the rate of alteration while remaining below the glass transition temperature, which has been estimated at ~725°C, thereby minimizing devitrification (Bender et al.,1978; Ryan and Sammis, 1981).

A powdered buffer assemblage (e.g., inset image, Fig. 3) containing magnetite and hematite (MH buffer) was used to buffer the experimental oxygen fugacity to approximately

Venus' surface fO_2. Powdered pyrite was added to produce SO_2 gas via the decomposition reaction:

$$FeS_{2(s)} + 2CO_{2(g)} \rightarrow Fe_{1-x}S_{(s)} + 2CO_{(g)} + SO_{2(g)}$$ (e.g., Figure 5 in Lv et al., 2015). (7)

Samples and buffer assemblages were placed in gold tubing and encased in a cold-seal pressure vessel (e.g., Fig. 3). The system was subsequently pressurized with pure CO_2 gas and heated to temperature for the pre-selected duration. At the conclusion of the runs, the buffer assemblages were checked to verify that magnetite, hematite, and pyrite remained, and thus were not exhausted over the duration of the runs.

Analytical Methods

Surface characterization using SEM (BSE and EDS)

Following each run, the surfaces of the samples were characterized using backscatter electron (BSE) images collected on the Phenom Pro scanning electron microscope (SEM) at the University of Tennessee, Knoxville, to assess the mineralogy and abundance of alteration products present. Specifically, each sample was imaged in a transect of 25 individual frames, each with a field of view of ~50 µm (Fig. 4). Phases (and aggregates of phases) in each image were then characterized using energy dispersive X-ray spectroscopy (EDS) and visual assessment of their morphologies and z-contrasts to determine their mineralogies. The percentages of surface area covered by the alteration phases were estimated by visually comparing them with a chart of modal abundances (e.g., Terry and Chilingar, 1955). Finally, the estimates from the 25 images were averaged to produce overall abundance estimates, expressed in percent, of the alteration phases for the samples. These surface analyses were useful to identify regions on the samples suitable for creating cross sections to be used in micro- and nano-scale analyses. To contrast the effect of the added SO_2 gas to the reactive environment, these steps were repeated using identical samples from a companion study (Teffeteller et al., 2020, 2021a, b) in which two sets of samples—VEN-4 (A and B) and VEN-5 (A and B)—were run for two weeks in pure CO_2, at MH fO_2 and 700°C and 470°C.

Cross section sample preparation (FIB)

The focused ion beam (FIB) *in-situ* milling and lift out technique was used to produce a microscale cross-section (foil) of the body of a sample, which allowed analyses of its surface and subsurface with minimal damage to the sample. The resultant foil is particularly suited to analyses using transmission electron microscopy (TEM), which employs analytical techniques that require samples to be electron transparent (i.e., ~80-100 nm thick; Wirth, 2009). Cross-sections for TEM analyses in this study were milled using the FEI Quanta 3D FEG instrument at Johnson Space Center, Houston, Texas.

Prior to milling, predetermined sites were located and assessed using BSE images generated from the FIB instrument's scanning electron microscope. Afterwards, a rectangle approximately 20 x 1.5 µm was projected on an image of the milling site, which defined the area on which a thin protective layer of carbon (e-beam carbon) ~0.8-1 µm was deposited using the instrument's carbon gas injection system (GIS) and electron beam, operating at 5 kV and 3.4 nA.

Given the fragility (Mohs hardness 2-3) of the anticipated sulfate phases, this extra step was taken to preserve surface phases during ion imaging and carbon cap deposition. The carbon cap, a larger, more robust ~3.5 µm thick and 30 µm long x 2.5 µm wide carbon layer, depicted in Figure 5, was subsequently deposited atop the first layer using the instrument's higher energy ion beam (i-beam carbon) operating at 30 kV, 100 pA, using the GIS. The carbon cap was deposited to armor the surface against ion bombardment and accidental damage during ion milling.

The milling process began with adjusting the operating conditions for the instrument to 30 kV, 15 nA and superimposing two larger rectangles or trapezoids ~30 x 16 µm on the image of the sample's surface on either side of the carbon cap. These regions were then bombarded by gallium ions, which milled away the sample material progressively deeper and created two "trenches" that achieved a final depth of ~10 µm on either side of the carbon cap (Fig. 6). These trenches permitted further milling—an undercut, a side-cut, and another partial side-cut, leaving a thin bridge of material connecting the cross-section to the sample body. This defined the initial cross-section dimensions, ~15 µm long x 6 µm deep x 3.5 µm thick. The tip of a manipulating needle was welded to the free edge of the new cross-section using platinum from the GIS, after which the cross-section was freed by completing the second side-cut. Then, the needle was used to lift the section out of the sample body, moving it to a TEM grid mounted adjacent to the sample. Thereafter, the section was welded to the grid and the connection between the tip of the needle and the section was milled away, allowing the needle to be removed. Using incrementally lower current, ion-milling continued, thinning and polishing both sides of the section to a final thickness of ~80-120 nm, appropriate for TEM analyses. Figure 7 shows a completed FIB section from VS-1B awaiting TEM analyses.

Section 4. Results

All experimental run products showed evidence of alteration, including surface deposition of alteration phases over all durations. Alteration products, including Ca- and Na-sulfates and Fe-oxides, were observed on both alkaline and tholeiitic starting compositions, although the amounts and sulfate mineralogies differed. Surface deposition of metallic phases occurred on all samples likely from metals that entered the vapor phase during experimentation (e.g., Beckman & Woodford, 1988; Berger et al., 2019), with nickel (Ni) and chromium (Cr) originating from the Waspaloy™ (58% Ni, 19% Cr, 13% Co, 4% Mo, 3% Ti, 1.4% Al) composition of the alloy plug and container. Gold (Au), silver (Ag), and platinum (Pt) were likely from the sample tubing and iron (Fe) from the decay of pyrite to pyrrhotite in the buffer assemblage.

Surface Alteration in the Presence of SO_2 Gas

Alkaline Basalts

At a run duration of 3 weeks at 470°C, 90 bars, the surface of sample VS-3A (Fig. 8A) was partially coated (40%) by thenardite as nearly uniform sized and evenly dispersed phases < 1 µm in diameter (Fig. 9B); isolated subhedral grains ~1–5 µm in diameter and aggregates of such grains, up to ~20 x 10 µm, covered another 1% of the sample. One instance of glauberite [$Na_2Ca(SO_4)_2$] was identified using EDS, occurring as a euhedral radial crystal mass. However, several regions (e.g., Fig. 9B, white arrows) on the surface exhibited distinct grain boundaries and showed no obvious evidence of reaction. EDS indicated these regions were olivine, pyroxene, and plagioclase microphenocrysts. Fe-oxides were rare (<<0.1%), randomly dispersed, submicron sized grains. Additionally, rare particles of Pt, Au, and Ag, indicated by EDS and their high z-contrast, were observed.

VS-4A, after reaction at 470°C, 90 bars for 4 weeks, (Fig. 8A) exhibited a 20% surface coating of evenly-dispersed, submicron scale phases, likely sulfates. The z-contrast and morphology were consistent with thenardite, though the grains were too small to resolve using EDS. Randomly distributed iron oxide phases <1–3 µm (Fig. 9C) covered 0.3% of the surface. Of the 20% total alteration phase coating, 98% consisted of sulfates and 2% of Fe-oxides, except on microphenocrysts of olivine, pyroxene, and plagioclase, where only rare nanoscale grains were observed. Siderite ($FeCO_3$) and magnesite ($MgCO_3$) were indicated in two instances—both occurring in surface vesicles. EDS spectra also suggested the presence of carbon in several transect analyses, though no other carbonate phase was identified. Minor Fe metal and Au were observed, suggesting possible reaction with the sample capsule material or experimental assemblage. Additionally, Ni-bearing phases were noted in several EDS analyses, often accompanied by minor sulfur concentrations. Other regions on the surface exhibited spectra consistent with pure silica and silica with alumina, though concentrations were not consistent with andalusite.

Thenardite dominated the alteration assemblage on the surface of VS-1A (700°C, 90 bars) at 70% coverage (Fig. 8B). Thenardite grains ranged in size from approximately 1 μm to > 30 μm in diameter with acicular, tabular, and prismatic habits that covered and obscured most of the surface (Fig. 9B). Acicular thenardite crystals ~1–5 μm long were thinly dispersed, however, coating microphenocrysts of olivine, pyroxene, and plagioclase (Fig. 9D). Iron oxides covered approximately 0.1% of the surface and occurred as randomly distributed grains < 1 μm in diameter.

Tholeiitic Basalts

VS-3B, reacted for 3 weeks at 470°C, 90 bars, exhibited scattered, discrete anhydrite grains that covered 0.1% of the surface. These larger acicular crystals, ~1–10 μm long, were encircled by a frosting of nanometer-sized phases of anhydrite that contributed 0.1% surface coverage (Figs. 8B and 10B). Fe-oxides (0.2%; Fig. 8B) were randomly distributed on the surface as single grains ≤ 1 μm, or in aggregate spheroid masses ~1–3 μm in diameter. Anhydrite and Fe-oxides contributed approximately equally to the alteration phase coverage on the sample.

After reaction at 470°C, 90 bars for 4 weeks, sample VS-4B exhibited a <<0.1% abundance of sulfate grains, ~2–4 μm in diameter (i.e., 3 discrete grains over the entire transect). Grains having z-contrast consistent with sulfates <1 μm in diameter covered <<0.1% of the surface (Fig. 8B). Fe-oxides (0.2%) were rare single grains <1 μm or were clustered with sulfates in heterophase aggregates 3–8 μm (Fig. 10C). Trace Ni associated with S was also present.

VS-1B, altered at 700°C, 90 bars for 2 weeks, was covered with a nearly-continuous (23.8%) frost-like coating of grains smaller than 1 μm (Figs. 8B and 10D), visually consistent with anhydrite, with ~6.2% of the surface covered by larger, twinned euhedral to subhedral anhydrite masses ranging from ~1–10 μm in diameter. Rare grains of Fe-oxide (0.8%) appeared either as isolated grains < 1 μm, as aggregates of such grains, or with anhydrite grains in heterophase clusters (Fig. 10D). Anhydrite contributed 97% of the alteration phase coverage and Fe-oxides 3%. Rare Au and Pt grains were observed. Examination of a FIB cross-section (Fig 7) of the specimen using z-contrast revealed a heterophase cluster composed of layered anhydrite, Fe-oxides, and possibly other non-silicates building from the surface. Prior to FIB milling, anhydrite and Fe-oxide grains had been identified in the cluster using EDS. The phase(s) underlying them were hidden, and therefore, not characterized. Abundant radial and dendritic spherulites populated the subsurface and formed a uniform near-surface layer <1 μm deep beneath nano-scale anhydrite and concentrated in a region beneath the anhydrite/Fe-oxide crystal mass. The nucleation of spherulites appeared to continue to a depth beyond the 6 μm depth of the FIB section. Unfortunately, TEM analyses were not conducted to determine the composition of the crystallites.

Surface Alteration in a Pure CO_2 Atmosphere at 90 Bars, MH fO_2

Alkaline basalts

SEM analyses of the surface of VEN-5A (470°C) revealed a 3% abundance of Fe-oxides and siderite ($FeCO_3$), occurring together in aggregates of grains less than 1 μm to >5 μm in diameter, which were thinly, but evenly, dispersed (Figs. 11 and 12A); however, grain

morphologies and sizes (≤ 1 μm) smaller than EDS spot size made them difficult to distinguish. Therefore, Fe-oxide and inferred siderite abundances were combined. Also observed were isolated Fe and Fe-Cr metal grains.

VEN-4A (700°C) exhibited a 0.2% abundance of Fe-oxides (Fig. 11) observed as rare discrete grains or clusters ≤ 1 μm in diameter (Fig. 12C). EDS analysis indicated that rare clusters contained possible siderite. Patches of Fe metal and Fe-Cr alloy, as well as rare deposits of Au and Pt metal were noted.

Tholeiitic basalts

After reaction at 470°C, VEN-5B abundances of Fe-oxides and siderite were 2% (Fig. 11) and occurred as small clusters (~1 μm) and aggregates of nanoscale phases that were distributed discontinuously on the glassy surface (Fig. 12B) and accumulated preferentially along cracks and ridges. Aggregate grain patches occasionally covered surface areas up to ~20 x 50 μm, and EDS analyses indicated greater abundances of siderite than those inferred on the other samples. Sporadic grains of a Fe-Cr metal were also present.

The surface of sample VEN-4B, which was reacted at 700°C, had a dominantly vitreous texture (Fig. 12D). SEM analyses determined that a coating of Fe-oxides and plausible siderite covered 0.1% of the sample (Fig. 11), appearing as randomly distributed clusters of grains < 1 μm to ~2 μm (Fig. 12D). Rare Fe metal and Fe-Cr alloy were also noted.

Section 5. Discussion

Run durations, temperatures, and basalt compositions were varied to contrast their effects on the mineralogies and abundances of alteration products in sulfur-bearing experiments. The surface coverages of total alteration products were then used to place qualitative constraints on alteration rates, and subsequently, Venus' surface ages. Analysis of the run products using identical samples reacted in pure CO_2 (Teffeteller et al. 2020, 2021a,b), afforded a further comparison with reaction in a SO_2-free reactive atmosphere. The production of sulfate phases in all SO_2-bearing experiments was consistent with both thermodynamic predictions (Fegley et al.,1997; Treiman, 2007; Zolotov, 2018; Simprech et al., 2020) and the results of other SO_2-basalt experiments (King et al., 2018; Palm et al., 2018; Renggli & King, 2018; Berger et al., 2019; Renggli et al., 2018, 2019), and confirmed the successful decomposition of pyrite to produce a sulfur-rich gas, likely SO_2. Interpretation of the mineralogy of alteration phases, including sub-micrometer sized grains, was based on the collective analysis of EDS spectra, grain morphology, and BSE z-contrast. All sample surfaces, including the CO_2 run products, exhibited a widely dispersed scattering of metal grains, similar to those described by Berger et al. (2019), that originated from gas interaction with parts of the experimental apparatus and the powdered buffer minerals.

SO_2-Bearing Experiments

Effect of Starting Composition on Reaction Products and Coverage

Alkaline and tholeiitic specimens were altered simultaneously in three experimental runs (i.e., VS-1, VS-3, and VS-4). In each run, independent of duration and temperature, reaction products were consistently more abundant on the alkaline composition (Fig. 8 and Table 5), 70% vs 27%, 40% vs 0.3%, and 20% vs 0.2%. Thenardite (Na_2SO_4) on all alkaline basalts comprised >99% of the total alteration phases, with Fe-oxides accounting for the remainder. Additionally, maximum sulfate grain sizes on alkali samples were larger than those on corresponding tholeiitic samples in all runs but VS-4 (A and B).

Though thenardite has been predicted and observed in previous work, it has not been suggested to be a major alteration product of basalt-SO_2 reactions (Fig. 9). However, its prevalence on alkaline samples suggests that the velocity of Na migration and resulting reaction rate in the alkaline glass are significantly more rapid than corresponding rates of Ca in the tholeiitic glass. This inference is consistent with the following principles (Fig.13A): **1)** SO_2 gas interaction with basalt glasses results in strong oxidation and chemical potential gradients that are drivers for diffusive migration of monovalent and divalent cations to the glass surface (King et al., 2018; Palm et al., 2018; Renggli & King, 2018; Berger et al., 2019; Renggli et al., 2018, 2019); **2)** diffusivity is a product of the diffusion coefficient of the cation and its concentration (Table 3) in the glass (Behrens 1992; Cooper et al. 1996); **3)** in silicate glasses ($An_{60}Ab_{40}$) analogous to basalts, Na has a relatively large diffusion coefficient (D_{Na}) and that $D_{Na} > D_{Ca} > D_{Mg}$ (Behrens, 1992); **4)** the availability of Na to react with SO_2 and form Na_2SO_4 on basalt glass is mediated by the glass's Fe^{3+}/Fe^{2+} and the participation of Na^{1+} in stabilizing network-forming Fe^{3+} during oxidation—Fe^{3+}/Fe^{2+} is governed by the equilibration fO_2 of the glass;

unreacted natural alkali specimens may have equilibrated substantially above QFM, in contrast to the tholeiitic specimens (Cook et al., 1990; Cooper et al., 1996; Renggli & King, 2018; Berger et al., 2019); and **5)** crystalline thenardite (53.34 cm^3 mol^{-1}) has a greater volume per mole than magnetite (44.53 cm^3 mol^{-1}), hematite (30.28 cm^3 mol^{-1}), siderite (29.38 cm^3 mol^{-1}) and anhydrite (45.94 cm^3 mol^{-1}) (Robie & Bethke, 1962) that likely facilitates efficient surface coverage of crystallizing thenardite. Moreover, because thenardite requires two moles of Na per mole of sulfate, rapid migration of Na from depth to the surface may engender greater crystal sizes and quantities.

However, grain sizes and abundances of sulfate reaction products on VS-4A (Fig. 9C) were less than those on the other alkali specimens. Reaction of CO_2 and SO_2 with the vessel over the extended duration may have changed the chemistry of the gases in the system, resulting in deposition of Ni, Fe, and C on the specimen surface. As gas composition was not monitored and the precise compositions of precipitant phases were not constrained, it is uncertain what caused this discrepancy. Pure crystalline thenardite has been shown to decompose in the presence of elemental carbon and a pure oxygen atmosphere, at a temperature of 500°C and ~1 bar pressure (Samadhi et al., 2003). A similar process may explain the lack of sulfate grains ≥1 μm observed on VS-4A. Testing this hypothesis would require more experimentation and the use of more precise analytical techniques, and therefore, falls outside of the scope of the present study.

The crystallinity of the alkali material permitted the additional assessment of concurrent mineral and glass alteration (Fig. 9). In high temperature oxidation experiments (Cutler et al., 2020; Filiberto et al., 2020), the rate of secondary hematite production was observed to be fastest on olivine phases, followed by glass. However, in the present SO_2-bearing experiments, microlites and microphenocrysts of olivine, pyroxene, and plagioclase phases exhibited zero to trace observable alteration products at 470°C (Fig.9B, C, D). Similarly, the original surface of VS-1A (700°C) was visible only where phases of olivine, plagioclase, and pyroxene were indicated. Matrix glass, on the other hand, was readily coated by sulfate phases in all three runs. Not only does this bimodal alteration exemplify the slower reaction of crystalline phases versus basaltic glass, but it also demonstrates that greater crystallinity in a basalt significantly slows the overall rate of surface sulfate production. A more crystalline alkali basalt may, therefore, appear "younger" via its emissivity spectra, than a glassier alkali basalt emplaced at the same time.

Anhydrite and Fe-oxides were produced in nearly equal trace amounts on tholeiitic samples (Fig. 8; VS-3B and VS-4B), which were run at Venus' surface temperature (470°C); only the high temperature run produced abundant anhydrite (26%). Heterophase masses of anhydrite and Fe-oxides (and possibly other phases) were observed on all reacted tholeiitic specimens, but none were detected on the alkaline surfaces. The production of anhydrite and Fe-oxide secondary phases supports both thermodynamic and experimental results in previous SO_2-basalt alteration studies (Barsukov et al., 1982; Surkov & Barsukov, 1985; Pieters et al., 1986; Fegley & Treiman, 1992; Treiman, 2007; Henley et al., 2015; King et al., 2018; Palm et al., 2018; Renggli & King, 2018; Berger et al., 2019; Renggli et al., 2018, 2019; Zolotov, 2018), but rates of alteration inferred here (0.05–0.13% per week) are far slower than rates in comparable alkali alteration runs (5–13% per week). Lower abundances, smaller grain sizes, and slower rates of reaction in the tholeiite run products may be explained by insufficient Na to charge-balance oxidizing Fe^{2+} to Fe^{3+} via inward diffusing electron holes (Fig.13A), which forces divalent cations to participate in the charge-balancing role (Cook et al., 1990; Cooper et al., 1996; Renggli & King, 2018) and results in nucleation of subsurface Fe-oxides and Na-, Fe-, and Mg-,

crystallites (Figure 7). As subsurface crystallization proceeds, it depletes Na, Fe, and Mg cations in the matrix glass, limiting their diffusion to the surface. Ca diffuses to the surface at a slower rate than that of Na to form modest amounts of anhydrite. The 700°C temperature increases the energy of the system and elevates the reaction rate, which produces greater amounts and larger grain sizes of anhydrite.

The co-crystallization and superposition of Fe-oxide on the surface of anhydrite grains indicate that Fe can diffuse through both the glass and anhydrite media to form surface oxides (Figs. 7 and 10). Dyar et al. (2020) propose that Venus' basaltic surfaces are likely coated by anhydrite ± calcite that decrease emissivity, and that hematite (Fe-oxides) has little to no effect. On the short timescales of the present study, however, Fe-oxides comprise a significant portion of the alteration assemblage on tholeiitic basalts. Therefore, it is possible that Fe-oxides make some contribution to VIRTIS emissivity contrasts.

Effect of Run Duration on Reaction Products and Coverage at 470°C, 90 Bars, and Magnetite-Hematite fO_2

Alkali basalt samples (VS-3A, and VS-4A) were altered over 22- and 30-day durations (Table 4). Minor Fe-oxides (0.2% and 0.02%, respectively) were observed on both alkali samples (Figs. 8 and 9B, C). However, as Fe-oxide quantities were less than 1% and grain sizes <1 μm, the effect that increased experimental duration had on Fe-oxide production is unclear, though their abundances decreased with time. Anhydrite has been predicted (Treiman, 2007; Zolotov, 2018) but it was not detected. Sulfate abundances and grain sizes were expected to increase with increasing duration; however, an increase was not observed (Fig. 8; Table 5). In addition to the evidence for the possible interaction of SO_2 gas with parts of the vessel, as previously discussed, the relatively low occurrence of sulfate phases on VS-4A may have been the result of the formation of an amorphous silica layer near the surface that inhibited further cation diffusion and reaction at the surface, as described in McCollum et al. (2013) and McCanta et al. (2014).

Tholeiite samples (VS-3B and VS-4B) retained much of their original vitreous surface textures (Fig. 10B, C), and had few alteration products overall (Fig. 8; Table 5). VS-4B was reacted concurrently with VS-4A. Therefore, lower secondary product abundances observed on the sample likely reflect reaction that was limited by interaction of SO_2 with parts of the experimental vessel, as well as the formation of a subsurface amorphous silica layer.

The effect of duration on reactions in these systems may be observable on longer time-scales than the 3- and 4-week experiments conducted here. However, alteration phase abundances in both sets of run products, when considered together, offer support to the hypothesis that chemisorption of SO_2 directly to the glass surface induces an instantaneous reaction with surface Na and Ca, producing an initially high abundance of sulfate phases, followed by far slower surface reactions governed by the diffusive transport mechanism (Henley et al., 2015; Renggli & King, 2018; Renggli et al., 2018). Therefore, sulfate product abundances generated in three weeks may not appear significantly different than those produced in four weeks of alteration, as depicted in Figure 9B and C.

Effect of Varying Run Temperature on Reaction Products and Coverage

Alkaline and tholeiitic samples (Figs. 8, 9, 10) were reacted in an SO_2-bearing CO_2 atmosphere under 90 bars pressure, near the MH fO_2 buffer at contrasting temperatures, 470°C for 22 days (VS-3A and VS-3B) and 700°C for 15 days (VS-1A and VS-1B) (Table 4). This is a 230°C difference in temperature, an increase of 49%. Though the run durations were not equal, it has been demonstrated above that reaction phenomena would be similar between 15- and 22-day runs at 470°C. As expected, the higher temperature exerted a more profound effect than run duration on alteration phase surface coverage and grain sizes on both basalt types that indicated higher diffusion rates; however, it had no discernable effect on alteration phase mineralogy. These results are consistent with the expectation that the 700°C temperature would increase the reaction rate beyond the rate at 470°C, and thereby provide a model of alteration over a duration beyond 4 weeks. In this context and after alteration, it was apparent that the crystal size of sulfate secondary phases was an important factor to discerning a rate of reaction, which would likely become rate-limiting as crystal growth proceeded. Renggli et al. (2019) presented textural evidence that both SO_2 gas and cations from the glass diffuse through a sulfate layer at the surface to engender further sulfate crystallization and create a gradually thickening continuous mineral crust. Crystal growth would eliminate the pore spaces in the sulfate coating that permit diffusion of SO_2, which would halt the chemical potential driver for cation diffusion. On both high temperature specimens, abundant sulfate grains ranging from <1–10 µm (VS-1B) and 1–30 µm (VS-1A) (Figs. 9D and 10D), suggest that such a threshold was not yet attained. It is, therefore, plausible that a crust of sulfate phases approaching ~30 µm or more in thickness can develop on altered basalts through which diffusion mechanics would continue to operate.

Alternatively, the abundance and large grain sizes of thenardite observed on the surface of the alkali sample (VS-1A) in the 700°C run are also consistent with reaction that exceeded the glass transition temperature, between ~630–725°C (Ryan & Sammis, 1981; Cooper et al., 1996). Devitrification of an identical alkali specimen reacted at 700°C by Teffeteller et al. (2020, 2021a, b) was attributed to surpassing the glass transition; however, without data from the subsurface, it is unclear whether this is the case for VS-1A. Using the same tholeiitic glass as VS-1B, in a 700°C run, Teffeteller et al. (2020, 2021a, b) showed that the subsurface remained glassy after alteration, which supported the suggestion of a higher glass transition temperature at ~725°C for tholeiitic basalts (Ryan & Sammis, 1981). Consequently, crystallites (Fig. 7) in the subsurface of the present 700°C run tholeiite glass (VS-1B) were not produced by exceeding the glass transition. Instead, they are interpreted as evidence for diffusive cation migration (Fig. 13) and subsurface nucleation of crystalline phases. This phenomenon occurs because the concentration of Na in the tholeiite glass is inadequate to charge-balance Fe^{2+} oxidizing to Fe^{3+} in the glass matrix (Cook et al., 1990; Cooper et al., 1996). The depth and abundance of the spherulites suggest that alteration proceeded to >6 µm into the glass interior. Depth of alteration and the abundance of spherulites would likely be less in the lower temperature run; however, as cross sections were not produced from 470°C run products, no comparison is possible.

Comparison between CO_2-only and CO_2+SO_2 experimental atmospheres

Surface reaction products on samples from two-week runs (470°C and 700°C) in pure CO_2, at MH buffer and 90 bars pressure (Fig. 11), were compared with three-week specimens from the present study to isolate the effect of added SO_2 to the reactive atmosphere. Fe-oxides were observed on all sets of run products (Figs. 8 and 11); however, they were generally less

abundant on the SO_2-bearing specimens. As predicted, sulfates were produced in the sulfur-bearing experiments. Siderite ($FeCO_3$) was also observed on the surfaces of CO_2 run products but was absent from the corresponding SO_2-bearing samples.

Abundances of alteration products on alkaline samples were significantly greater in the sulfur-bearing runs at both temperatures (Fig. 8). Here, it is proposed that this is the result of instantaneous reaction with Na cations at the surface via SO_2 chemisorption, followed by rapid migration of network modifying cations from the interior outward, compelled by both redox and chemical potential gradients created by the reactive gases (Fig. 13A). Na has a greater diffusivity in glass than the other network-modifying cations, as detailed in the prior discussion of the effects of starting composition. Na was sufficient to stabilize Fe^{3+} in the glass matrix, freeing it to diffuse rapidly to the surface of the glass where it reacted with SO_2 to form thenardite.

Tholeiite-sulfur run products at 470°C were fewer (~0.4%) compared with 2% on the CO_2 only specimen (Figs. 8 and 11). At 700°C, tholeiite reaction products were far greater (~30%) on the SO_2-bearing sample than the CO_2 sample (0.7%). As described in the discussion of the effects of starting composition, SO_2 was adsorbed onto the glass, as with the alkali specimens, and reacted instantaneously with Ca and Na to form a surface layer of nano-scale sulfate phases (Figure 10B and D); however, the lower concentration of Na was largely consumed to stabilize oxidizing Fe (Table 3; Fig 13A). The nucleation of crystallites within the glass slowed cation diffusion to the surface. The higher temperature specimen, VS-1B, shows that the concentration of Ca may be sufficient to overcome these barriers to diffusion toward the surface of the glass over time.

Figure 13A and B depict similar reaction mechanics in a pure CO_2 atmosphere. The key difference is the absence of the chemical potential gradient imposed by SO_2. Without which, reaction via oxidation likely proceeds at a slower rate, as seen in the grain sizes and quantities of run products from the pure CO_2 runs (Figs. 10 and 11), compared with SO_2-bearing run products (Figs. 8 and 9). Further support is found by comparing the depth of alteration of both SO_2-bearing and pure CO_2 tholeiitic run products that were altered at 700°C for two weeks: >6 µm (SO_2) versus 23 nm (CO_2). It is notable that reaction product abundances were slightly greater in the lower temperature, pure CO_2 run. However, this is attributable to the production of siderite that is likely metastable at the run conditions (Koziol, 2004), but not stable at 700°C. If SO_2 is ephemeral at the Venus surface, then siderite may be a significant alteration phase on basalt surfaces.

Alteration Rates and Venus' Surface Age Constraints

Alteration rates, as suggested by VIRTIS emissivity variations and based on the experimental oxidation of olivine crystals and glassy basaltic materials, have been used to constrain the ages of volcanic features on the Venus surface to 2.5 Ma–250,000 years (Smrekar et al., 2010), or to ~3,000–11,000 years (Teffeteller et al. 2021a, b), or to perhaps a few months to years old (Cutler et al., 2020; Filiberto et al., 2020), depending on the composition of the solid and the kinetic model used. Elevated 1 µm emissivity variations correlate with high total Fe^{2+} content in silicate materials (Smrekar et al., 2010; Stofan et al., 2016; Gilmore et al., 2017; D'Incecco et al., 2017; Dyar et al., 2020; Filiberto et al., 2020; Mueller et al., 2020; Helbert et

al., 2021), and alteration changes the glass structure at depth (e.g., Fig 13), and creates divalent and monovalent cation- depleted regions and Si-rich regions in the subsurface (Cook et al., 1990; Cooper et al., 1996; McCanta et al., 2014; Henley et al., 2015; King et al., 2018; Renggli & King, 2018; Berger et al., 2019; Renggli et al. 2018, 2019; Teffeteller et al., 2020, 2021a, b). Surface alteration products and the subsurface chemical layers serve as an alteration rind that acts to obscure unaltered, FeO-rich glass beneath them, thereby reducing emissivity (Smrekar et al., 2010; Stofan et al., 2016; Dyar et al., 2020; Helbert et al., 2021). Alteration thickness in the subsurface of a silicate glass is predicted to be proportional to the square root of time (Cook et al., 1990; Cooper et al., 1996). Teffeteller et al. (2021a, b) used the depth of alteration from experimentation and a target depth of alteration between 5 and 10 µm—excluding surface grains—to calculate their rates. The tholeiitic glass showed a slightly deeper alteration front than the alkaline composition (16 vs 12 nm). Consequently, the calculated rate for alkali basalts was 880 $nm^2\ yr^{-1}$ and tholeiite basalts was 1600 $nm^2\ yr^{-1}$. However, it is unclear whether the same parabolic relationship governs surface alteration mineral accumulation.

A coating of hematite on Venus' surface rocks has been suggested as the source of VIRTIS emissivity excursions at Idunn Mons (Fig. 2) and other volcanic landforms (Smrekar et al., 2010; Stofan et al., 2016; Gilmore et al., 2017; D'Incecco et al., 2017; Cutler et al., 2020; Filiberto et al., 2020; Mueller et al., 2020; Teffeteller et al., 2020, 2021a, b). In oxidation studies using basalt and mafic minerals reacted over several experimental durations (Cutler et al., 2020; Filiberto et al., 2020), VNIR reflectance spectra changed due to a progressively more abundant coating of nanophase hematite. The resultant rates of hematite coverage were then used to proposed that the anomalous VIRTIS emissivity at Idunn Mons was consistent with basalt that was no more than a few years old. However, if Venus' surface is interacting with its atmospheric SO_2, as indicated in Venera 13–14 and Vega 2 XRF analyses (Surkov & Barsukov, 1985), then clearly oxidation is not the sole alteration mechanism.

Instead, results here corroborate declarations made in other SO_2 gas-solid experimental studies that sulfate alteration products likely coat basaltic rocks on the Venus surface (King et al., 2018; Palm et al., 2018; Renggli & King, 2018; Berger et al., 2019; Renggli et al., 2018, 2019). It has been proposed that the initial rapid surface reaction rate may be linear, which is followed by a parabolic reaction rate (Renggli et al., 2018). The specimens here exhibit surface products consistent with that inference (Figs. 9 and 11). However, it is not clear from the present run products how long the initial period lasts. As their alteration layer thicknesses are unknown, parabolic reaction rates are not presented. Dyar et al. (2020) demonstrate that a coating of sulfate minerals would have a modest reducing effect on emissivity spectra that would require a sufficiently thick crust (~30 µm) of secondary sulfate coatings to justify the thermal anomaly observed by VIRTIS spectrometers on Venus' Idunn Mons. The results of the present study demonstrate that the rate to produce such a coating at Venus conditions is strongly influenced by the composition of the primary basalt.

On tholeiitic specimens reacted at 470°C, discontinuous grains and grain aggregates of anhydrite and Fe-oxides approach 5–10 µm covering ~0.4% of the surface after 3 weeks of alteration. If alteration is continuous, then the entire surface could be covered in less than 20 years. A coating approaching 30 µm may then accumulate in as few as ~60 years. Time scales would be longer, assuming a parabolic alteration rate. If the Fe-oxides are hematite, then a thinner crust of heterophase anhydrite and hematite may be sufficient. Nonetheless, a 30 µm thick alteration mineral crust may form in less than 5 months on the same tholeiite at 700°C. At

Venus' surface temperature, this scenario is unlikely, but it is suggestive that significant alteration may occur on tholeiitic basalts on timescales of less than 60 years.

Thenardite, which has similar optical properties to anhydrite, was ubiquitous on the surfaces of all altered alkaline specimens. Glassy alkaline basalts developed coatings of thenardite with grain sizes up to >5 μm covering 40% of the surface in 3 weeks at 470°C. Therefore, if reaction is continuous, then it is likely that a coating of several tens of microns thick could advance over the surface of similar alkaline basaltic material within 2–3 months. Alteration of the alkali specimen at 700°C yielded a nearly complete reaction phase rind that occurred in only 15 days. Moreover, grain sizes ranged up to 30 μm in diameter. Though this temperature is much higher than Venus' surface, the 700°C specimen suggests it is possible that alkali basalts on the planet may produce a ~30 μm thenardite coating in a few weeks to a few months.

Chemical weathering may proceed very quickly on either basalt composition on the Venus surface, which may produce sufficiently thick rinds of sulfate to reduce observable emissivity within months to decades. The atmospheric concentration of SO_2 is ~150 ppm and reaction products and rates observed here are consistent with results reported by Berger et al. (2019) using 140 ppm and 320 ppm dry SO_2, under nearly identical *T*, *P*, and fO_2 conditions; however, reactions on Venus are dependent upon a near-surface SO_2 concentration that is currently unconstrained (Zolotov, 2018). Moreover, the results reported here assume that concentrations of atmospheric SO_2 are relatively constant at the near-surface. If so, the strong contrast of alteration rates could be used to crudely estimate primary rock compositions. Fluxes of SO_2 that dissipate over time, however, have been observed in Venus' atmosphere, similar to volcanic activity-related pulses documented on Earth (Esposito, 1984; Glaze, 1999; Marcq et al., 2012). If SO_2 concentrations are more transient at the surface as a result, then alteration rates would likely be variable, especially proximal to the source.

Section 6. Summary

The opaque Venus atmosphere impedes comprehensive spectroscopy of its surface (Esposito, 1984; Moroz, 2002). However, VIRTIS spectral observations of its surface have revealed variations in thermal emissivity that suggest different degrees of chemical weathering, though without compositional data (Smrekar et al., 2010). Interpretation of emissivity relies on an understanding of the mineralogy of the weathering products and the rate at which the rocks are altering. Several experimental studies using sulfur-free gases and analogous basaltic materials have predicted Venus' altered rocks are coated by hematite and have yielded reaction rates that suggest its unweathered volcanic features, such as lava flows on the steep-sided dome and flanks of Idunn Mons, may have been emplaced between 2.5 m.y. to just a few months before observation (Smrekar et al., 2010; Cutler et al., 2020; Filiberto et al. 2020; Teffeteller et al., 2020, 2021a, b). Yet, alteration of Venus' basaltic rocks likely involves chemical interaction with is atmospheric SO_2, which has been demonstrated in thermodynamic and other experimental works to readily alter basaltic rocks and produce sulfate and Fe-oxide reaction products (Barsukov et al., 1982; Surkov & Barsukov, 1985; Treiman, 2007; Filiberto, 2014; King et al., 2018; Palm et al., 2018; Renggli & King, 2018; Zolotov, 2018; Berger et al., 2019; Renggli et al., 2018, 2019; Dyar et al., 2020; Simprech et al., 2020). Nevertheless, rates of alteration and the mineralogy of reaction products likely to be coating Venus' rocks remain unconstrained.

In the present work, glassy tholeiitic and alkaline basaltic specimens were reacted in SO_2-bearing CO_2 atmospheres at temperatures, pressure, and fO_2 relevant to the Venus surface. Alteration phase mineralogy and abundances crystallizing on the specimens were characterized using backscatter electron imaging and energy dispersive X-ray spectroscopy techniques. Results from the altered specimens were compared with run products that were reacted in identical conditions in pure CO_2. Alteration rates were then estimated and used to interpret the age of fresh basaltic features on Idunn Mons.

In the presence of SO_2, reaction products and rates were strongly influenced by the starting composition of the substrate. Anhydrite and minor Fe-oxides crystallized on tholeiitic run products. Alkali specimens were coated by larger, more abundant thenardite grains and trace Fe-oxides. Grain sizes and abundances were consistent with a continual flux of Na, Ca, and Fe cations diffusing from the interior of the specimens to their surfaces, although direct observation of the characteristic chemical layering could not be observed. Moreover, the chemical behavior of Na was recognized in the tholeiite glass as a charge compensator in Fe^{2+} to Fe^{3+} oxidation, and in the alkali glass as the prevalent diffusive cation when charge compensation was satisfied.

When run products were compared to those reacted in pure CO_2, it is proposed that alteration rates were increased due to the additional chemical potential gradient imposed by SO_2 that increased diffusion rates, as evidenced by more abundant, larger-grained reaction products, and possibly greater depth of alteration into basalt glasses. Furthermore, it was observed that primary rock compositions may be crudely inferred by their contrasting rates of reaction in a SO_2-bearing atmosphere. This distinction does not seem likely in a sulfur-free atmosphere.

Alteration rates, as estimated by how efficiently alteration products coated the reacted specimens, were greater (5–35% per week) in the alkali glass, versus the tholeiite glass (0.05–15% per week). Thus, depending on their composition, the fresh basalts observed on Idunn Mons may have been only a few weeks to <100 years old when they were first recognized. These suggested ages are somewhat speculative as they do not assume a parabolic rate of alteration, nor do they account for the time for a sufficiently thick alteration crust to form (~30 μm) that would decrease emissivity contrast. Therefore, the rates and ages suggested here may be understood as lower bounds.

Section 7. Future Work

The present study places constraints on the products and rates of chemical interactions between basaltic materials and SO_2-bearing reactive atmospheres like those found on the Venus surface. It is a component of a broader work with the goal of using experimental results that model weathering phenomena on Venus to inform interpretations of remote sensing properties from its surface. As nanoscale TEM analyses used to characterize the depths of alteration fronts and product mineralogies in the subsurface of reacted basalts could not be conducted in the present study, future work is needed to complete such analyses. Furthermore, to understand the effect of duration on alteration product growth in both grain size and surface coverage, and to test the hypothesis that the reaction rate follows a parabolic function, future work should include additional incremental (e.g., 1- and 2-week) experiments to complete a time series. An estimate of the time to achieve a 30 µm reaction rind may also result from time series experiments. However, consideration should be made to changing the experimental setup to use reactor materials (if such materials exist) that are less susceptible to reaction with SO_2-bearing gases, in view of the results from the 4-week run presented here. It would be beneficial to explore an experimental apparatus design that may: simulate Venus' surface temperature, pressure, and fO_2; permit direct insertion of reactive gases and allow for their concentrations to be monitored and regulated; accommodate samples large enough for spectral analyses; allow for reactions to be observed in real time. Additional work to compare alteration of solely synthetic glasses, and separately, only natural basalts would be useful to eliminate the possible effects of crystalline phases, surface roughness, and vesicularity present in the natural alkaline samples used here.

The results of this study suggest that sulfate grain sizes and alteration rind thicknesses likely increase more quickly than the depth of subsurface alteration fronts in basaltic glasses. Dyar et al. (2020) proposed that such coatings that grow to an estimated 30 µm may sufficiently obscure the surfaces of primary basaltic rocks that can explain VIRTIS emissivity variations discussed in Smrekar et al. (2010). It is also shown that crystalline constituents in basalts develop alteration phases more slowly than glasses. Further work, therefore, is needed to measure how anhydrite and thenardite crusts of variable thickness on basaltic glasses and mafic minerals affect 470°C VNIR emissivity and radar reflectance spectra. The resultant data, synthesized with the alteration rates suggested in the present work, will aid in interpretation of VIRTIS data and future emissivity data collected by spectrometers on NASA's VERITAS and Davinci + orbiters and ESA's Envision spacecraft that could further constrain the ages of the Venus surface and inform prospective selection of site for *in-situ* analyses. Moreover, the visible spectrum optical properties of thenardite and anhydrite encrusted basalts (and granites/rhyolites) should be explored for accurate interpretations of Venus' tesserae terrains using images taken by the Davinci + descent probe.

List of References

Barsukov, V. L., Volkov, V. P., & Khodakovsky, I. L. (1982). The crust of Venus: Theoretical models of chemical and mineral composition. *Journal of Geophysical Research*, *87*(S01), A3. https://doi.org/10.1029/jb087is01p000a3

Basilevsky, A. T., Ivanov, M. A., Head, J. W., Aittola, M., & Raitala, J. (2007). Landing on Venus: Past and future. *Planetary and Space Science*, *55*(14), 2097–2112. https://doi.org/10.1016/j.pss.2007.09.005

Beckman, J. P., & Woodford, D. A. (1988). Intergranular Sulfur Attack in Nickel and Nickel-Base Alloys. *Proceedings of the Sixth International Symposium on Superalloys Sponsored by the High Temperature Alloys Committee of the Metallurgical Society, Held September 18–22, 1988*, 795–804. https://www.tms.org/Superalloys/10.7449/1988/Superalloys_1988_795_804.pdf

Behrens, H. (1992). Na and Ca tracer diffusion in plagioclase glasses and supercooled melts. *Chemical Geology*, *96*(3–4), 267–275. https://doi.org/10.1016/0009-2541(92)90058-d

Bender, J. F., Hodges, F. N., & Bence, A. E. (1978). Petrogenesis of basalts from the project FAMOUS area: experimental study from 0 to 15 kbars. *Earth and Planetary Science Letters*, *41*(3), 277–302. https://doi.org/10.1016/0012-821x(78)90184-x

Berger, G., Cathala, A., Fabre, S., Borisova, A. Y., Pages, A., Aigouy, T., Esvan, J., & Pinet, P. (2019). Experimental exploration of volcanic rocks-atmosphere interaction under Venus surface conditions. *Icarus*, *329*, 8–23. https://doi.org/10.1016/j.icarus.2019.03.033

Bézard, B., & de Bergh, C. (2007). Composition of the atmosphere of Venus below the clouds. *Journal of Geophysical Research*, *112*(E4), n/a. https://doi.org/10.1029/2006je002794

Carlson, R. W., Baines, K. H., Encrenaz, T. H., Taylor, F. W., Drossart, P., Kamp, L. W., Pollack, J. B., Lellouch, E., Collard, A. D., Calcutt, S. B., Grinspoon, D., Weissman, P. R., Smythe, W. D., Ocampo, A. C., Danielson, G. E., Fanale, F. P., Johnson, T. V., Kieffer, H. H., Matson, D. L., … Soderblom, L. A. (1991). Galileo Infrared Imaging Spectroscopy Measurements at Venus. *Science*, *253*(5027), 1541–1548. https://doi.org/10.1126/science.253.5027.1541

Cook, G. B., Cooper, R. F., & Wu, T. (1990). Chemical diffusion and crystalline nucleation during oxidation of ferrous iron-bearing magnesium aluminosilicate glass. *Journal of Non-Crystalline Solids*, *120*(1–3), 207–222. https://doi.org/10.1016/0022-3093(90)90205-z

Cooper, R. F., Fanselow, J. B., & Poker, D. B. (1996). The mechanism of oxidation of a basaltic glass: Chemical diffusion of network-modifying cations. *Geochimica et Cosmochimica Acta*, *60*(17), 3253–3265. https://doi.org/10.1016/0016-7037(96)00160-3

Crank, J. (1980). *The Mathematics of Diffusion (Oxford Science Publications)* (2nd ed.). Oxford University Press.

Cutler, K. S., Filiberto, J., Treiman, A. H., & Trang, D. (2020). Experimental Investigation of Oxidation of Pyroxene and Basalt: Implications for Spectroscopic Analyses of the Surface of Venus and the Ages of Lava Flows. *The Planetary Science Journal*, *1*(1), 21. https://doi.org/10.3847/psj/ab8faf

D'Incecco, P., Müller, N., Helbert, J., & D'Amore, M. (2017). Idunn Mons on Venus: Location and extent of recently active lava flows. *Planetary and Space Science*, *136*, 25–33. https://doi.org/10.1016/j.pss.2016.12.002

Dyar, M. D., Helbert, J., Cooper, R. F., Sklute, E. C., Maturilli, A., Mueller, N. T., Kappel, D., & Smrekar, S. E. (2020). Surface weathering on Venus: Constraints from kinetic, spectroscopic, and geochemical data. *Icarus*, 114139. https://doi.org/10.1016/j.icarus.2020.114139

Esposito, L. W. (1984). Sulfur Dioxide: Episodic Injection Shows Evidence for Active Venus Volcanism. *Science*, *223*(4640), 1072–1074. https://doi.org/10.1126/science.223.4640.1072

Fegley, B., Klingelhöfer, G., Brackett, R. A., Izenberg, N., Kremser, D. T., & Lodders, K. (1995). Basalt Oxidation and the Formation of Hematite on the Surface of Venus. *Icarus*, *118*(2), 373–383. https://doi.org/10.1006/icar.1995.1197

Fegley, B., & Prinn, R. G. (1989). Estimation of the rate of volcanism on Venus from reaction rate measurements. *Nature*, *337*(6202), 55–58. https://doi.org/10.1038/337055a0

Fegley, B., Zolotov, M. Y., & Lodders, K. (1997). The Oxidation State of the Lower Atmosphere and Surface of Venus. *Icarus*, *125*(2), 416–439. https://doi.org/10.1006/icar.1996.5628

Filiberto, J. (2014). Magmatic diversity on Venus: Constraints from terrestrial analog crystallization experiments. *Icarus*, *231*, 131–136. https://doi.org/10.1016/j.icarus.2013.12.003

Filiberto, J., Trang, D., Treiman, A. H., & Gilmore, M. S. (2020). Present-day volcanism on Venus as evidenced from weathering rates of olivine. *Science Advances*, *6*(1), eaax7445. https://doi.org/10.1126/sciadv.aax7445

Gilmore, M., Treiman, A., Helbert, J., & Smrekar, S. (2017). Venus Surface Composition Constrained by Observation and Experiment. *Space Science Reviews*, *212*(3–4), 1511–1540. https://doi.org/10.1007/s11214-017-0370-8

Gilmore, M. S., Mueller, N., & Helbert, J. (2015). VIRTIS emissivity of Alpha Regio, Venus, with implications for tessera composition. *Icarus*, *254*, 350–361. https://doi.org/10.1016/j.icarus.2015.04.008

Glaze, L. S. (1999). Transport of SO_2 by explosive volcanism on Venus. *Journal of Geophysical Research: Planets*, *104*(E8), 18899–18906. https://doi.org/10.1029/1998je000619

Hashimoto, G. L. and Sugita, S. (2003). On observing the compositional variability of the surface of Venus using nightside near-infrared thermal radiation. *Journal of Geophysical Research*, *108*(E9), 1–8. https://doi.org/10.1029/2003je002082

Head, J. W., Crumpler, L. S., Aubele, J. C., Guest, J. E., & Saunders, R. S. (1992). Venus volcanism: Classification of volcanic features and structures, associations, and global distribution from Magellan data. *Journal of Geophysical Research*, *97*(E8), 13153. https://doi.org/10.1029/92je01273

Helbert, J., Maturilli, A., Dyar, M. D., & Alemanno, G. (2021). Deriving iron contents from past

and future Venus surface spectra with new high-temperature laboratory emissivity data. *Science Advances*, *7*(3), eaba9428. https://doi.org/10.1126/sciadv.aba9428

Henley, R. W., King, P. L., Wykes, J. L., Renggli, C. J., Brink, F. J., Clark, D. A., & Troitzsch, U. (2015). Porphyry copper deposit formation by sub-volcanic sulphur dioxide flux and chemisorption. *Nature Geoscience*, *8*(3), 210–215. https://doi.org/10.1038/ngeo2367

Kane, S. R., Arney, G., Crisp, D., Domagal-Goldman, S., Glaze, L. S., Goldblatt, C., Grinspoon, D., Head, J. W., Lenardic, A., Unterborn, C., Way, M. J., & Zahnle, K. J. (2019). Venus as a Laboratory for Exoplanetary Science. *Journal of Geophysical Research: Planets*, *124*(8), 2015–2028. https://doi.org/10.1029/2019je005939

Kappel, D., Arnold, G., & Haus, R. (2016). Multi-spectrum retrieval of Venus IR surface emissivity maps from VIRTIS/VEX nightside measurements at Themis Regio. *Icarus*, *265*, 42–62. https://doi.org/10.1016/j.icarus.2015.10.014

King, P. L., Wheeler, V. M., Renggli, C. J., Palm, A. B., Wilson, S. A., Harrison, A. L., Morgan, B., Nekvasil, H., Troitzsch, U., Mernagh, T., Yue, L., Bayon, A., DiFrancesco, N. J., Baile, R., Kreider, P., & Lipiński, W. (2018). Gas–Solid Reactions: Theory, Experiments and Case Studies Relevant to Earth and Planetary Processes. *Reviews in Mineralogy and Geochemistry*, *84*(1), 1–56. https://doi.org/10.2138/rmg.2018.84.1

Koziol, A. M. (2004). Experimental determination of siderite stability and application to Martian Meteorite ALH84001. *American Mineralogist*, *89*(2–3), 294–300. https://doi.org/10.2138/am-2004-2-306

Lv, W., Yu, D., Wu, J., Zhang, L., & Xu, M. (2015). The chemical role of CO_2 in pyrite thermal decomposition. *Proceedings of the Combustion Institute*, *35*(3), 3637–3644. https://doi.org/10.1016/j.proci.2014.06.066

Marcq, E., Bertaux, J.-L., Montmessin, F., & Belyaev, D. (2012). Variations of sulphur dioxide at the cloud top of Venus's dynamic atmosphere. *Nature Geoscience*, *6*(1), 25–28. https://doi.org/10.1038/ngeo1650

McCammon, C. (2005). Geochemistry: The Paradox of Mantle Redox. *Science*, *308*(5723), 807–808. https://doi.org/10.1126/science.1110532

McCanta, M. C., Dyar, M. D., & Treiman, A. H. (2014). Alteration of Hawaiian basalts under sulfur-rich conditions: Applications to understanding surface-atmosphere interactions on Mars and Venus. *American Mineralogist*, *99*(2–3), 291–302. https://doi.org/10.2138/am.2014.4584

McCollom, T. M., Robbins, M., Moskowitz, B., Berquó, T. S., Jöns, N., & Hynek, B. M. (2013). Experimental study of acid-sulfate alteration of basalt and implications for sulfate deposits on Mars. *Journal of Geophysical Research: Planets*, *118*(4), 577–614. https://doi.org/10.1002/jgre.20044

Moroz, V. I. (2002). Estimates of visibility of the surface of Venus from descent probes and balloons. *Planetary and Space Science*, *50*(3), 287–297. https://doi.org/10.1016/s0032-0633(01)00128-3

Mueller, N., Helbert, J., Hashimoto, G. L., Tsang, C. C. C., Erard, S., Piccioni, G., & Drossart, P.

(2008). Venus surface thermal emission at 1μm in VIRTIS imaging observations: Evidence for variation of crust and mantle differentiation conditions. *Journal of Geophysical Research*, *113*. https://doi.org/10.1029/2008je003118

Mueller, N. T., Smrekar, S., Helbert, J., Stofan, E., Piccioni, G., & Drossart, P. (2017). Search for active lava flows with VIRTIS on Venus Express. *Journal of Geophysical Research: Planets*, *122*(5), 1021–1045. https://doi.org/10.1002/2016je005211

Mueller, N. T., Smrekar, S. E., & Tsang, C. C. C. (2020). Multispectral surface emissivity from VIRTIS on Venus Express. *Icarus*, *335*, 113400. https://doi.org/10.1016/j.icarus.2019.113400

Nimmo, F., & McKenzie, D. (1998). Volcanism and tectonics on Venus. *Annual Review of Earth and Planetary Sciences*, *26*(1), 23–51. https://doi.org/10.1146/annurev.earth.26.1.23

Palm, A. B., King, P. L., Renggli, C. J., Hervig, R. L., Dalby, K. N., Herring, A., Mernagh, T. P., Eggins, S. M., Troitzsch, U., Beeching, L., Kinsley, L., & Guagliardo, P. (2018). Unravelling the Consequences of SO_2–Basalt Reactions for Geochemical Fractionation and Mineral Formation. *Reviews in Mineralogy and Geochemistry*, *84*(1), 257–283. https://doi.org/10.2138/rmg.2018.84.7

Pieters, C. M. (1983). Strength of mineral absorption features in the transmitted component of near-infrared reflected light: First results from RELAB. *Journal of Geophysical Research: Solid Earth*, *88*(B11), 9534–9544. https://doi.org/10.1029/jb088ib11p09534

Pieters, C. M., Head, J. W., Pratt, S., Patterson, W., Garvin, J., Barsukov, V. L., Basilevsky, A. T., Khodakovsky, I. L., Selivanov, A. S., Panfilov, A. S., Gektin, Y. U. M., & Narayeva, Y. M. (1986). The Color of the Surface of Venus. *Science*, *234*(4782), 1379–1383. https://doi.org/10.1126/science.234.4782.1379

Renggli, C. J., & King, P. L. (2018). SO_2 Gas Reactions with Silicate Glasses. *Reviews in Mineralogy and Geochemistry*, *84*(1), 229–255. https://doi.org/10.2138/rmg.2018.84.6

Renggli, C. J., King, P. L., Henley, R. W., Guagliardo, P., McMorrow, L., Middleton, J. P., & Turner, M. (2018). An experimental study of SO_2 reactions with silicate glasses and supercooled melts in the system anorthite–diopside–albite at high temperature. *Contributions to Mineralogy and Petrology*, *174*(1), 1–19. https://doi.org/10.1007/s00410-018-1538-2

Renggli, C. J., Palm, A. B., King, P. L., & Guagliardo, P. (2019). Implications of Reactions Between SO_2 and Basaltic Glasses for the Mineralogy of Planetary Crusts. *Journal of Geophysical Research: Planets*, *124*(10), 2563–2582. https://doi.org/10.1029/2019je006045

Robie, R. A., & Bethke, P. M. (1962). Molar volumes and densities of minerals. *Report: Trace Elements Investigations*, *822*, 1–30. https://doi.org/10.3133/70159012

Ryan, M. P., & Sammis, C. G. (1981). The glass transition in basalt. *Journal of Geophysical Research: Solid Earth*, *86*(B10), 9519–9535. https://doi.org/10.1029/jb086ib10p09519

Samadhi, T. W., Jones, L. E., & Clare, A. G. (2003). Influence of Carbon on SOxEmissions from Glass Processing. *Journal of the American Ceramic Society*, *86*(12), 2044–2049.

https://doi.org/10.1111/j.1151-2916.2003.tb03606.x

Seiff, A., Schofield, J. T., Kliore, A. J., Taylor, F. W., Limaye, S. S., Revercomb, H. E., Sromovsky, L. A., Kerzhanovich, V. V., Moroz, V. I., & Marov, M. Y. (1985). Models of the structure of the atmosphere of Venus from the surface to 100 kilometers altitude. *Advances in Space Research*, *5*(11), 3–58. https://doi.org/10.1016/0273-1177(85)90197-8

Semprich, J., Filiberto, J., & Treiman, A. H. (2020). Venus: A phase equilibria approach to model surface alteration as a function of rock composition, oxygen- and sulfur fugacities. *Icarus*, *346*, 113779. https://doi.org/10.1016/j.icarus.2020.113779

Skjelkvåle, B.-L., Amundsen, H. E. F., O'Reilly, S. Y., Griffin, W. L., & Gjelsvik, T. (1989). A primitive alkali basaltic stratovolcano and associated eruptive centres, Northwestern Spitsbergen: Volcanology and tectonic significance. *Journal of Volcanology and Geothermal Research*, *37*(1), 1–19. https://doi.org/10.1016/0377-0273(89)90110-8

Smrekar, S. E., Stofan, E. R., Mueller, N., Treiman, A., Elkins-Tanton, L., Helbert, J., Piccioni, G., & Drossart, P. (2010). Recent Hotspot Volcanism on Venus from VIRTIS Emissivity Data. *Science*, *328*(5978), 605–608. https://doi.org/10.1126/science.1186785

Smrekar, S.E., Stofan, E.R., & Mueller, N. (2014). Venus: surface and interior, in *Encyclopedia of the Solar System*, ed. by Spohn, T., Breuer, D., & Johnson, T.V. *Elsevier*, *3*, 323–341

Stofan, E. R., Smrekar, S. E., Mueller, N., & Helbert, J. (2016). Themis Regio, Venus: Evidence for recent (?) volcanism from VIRTIS data. *Icarus*, *271*, 375–386. https://doi.org/10.1016/j.icarus.2016.01.034

Surkov, Y. A., & Barsukov, V. L. (1985). Composition, structure and properties of Venus rocks. *Advances in Space Research*, *5*(8), 17–29. https://doi.org/10.1016/0273-1177(85)90237-6

Taylor, F., & Grinspoon, D. (2009). Climate evolution of Venus. *Journal of Geophysical Research*, *114*, n/a. https://doi.org/10.1029/2008je003316

Teffeteller, H., Filiberto, J., McCanta, M.C., Treiman A.H., Keller, L., Cherniak, D., and Rutherford, M. (2020), Experimental study of the alteration of basalt on the surface of Venus: Houston, Texas, Lunar and Planetary Science LI abstract #2038

Teffeteller, H., Filiberto, J., McCanta, M.C., Treiman A.H., Keller, L., Cherniak, D., and Rutherford, M. (2021a), Experimental study of the alteration of basalt on the surface of Venus: Houston, Texas, Lunar and Planetary Science LII abstract #1635

Teffeteller, H., Filiberto, J., McCanta, M.C., Treiman A.H., Keller, L., Cherniak, D., Rutherford, M., Cooper, R.F. (2021b), Experimental study of the alteration of basalt on the surface of Venus. *Icarus (In revision)*

Terry, R. D., & Chilingar, G. V. (1955). Summary of "Concerning some additional aids in studying sedimentary formations," by M. S. Shvetsov. *Journal of Sedimentary Research*, *25*(3), 229–234. https://doi.org/10.1306/74d70466-2b21-11d7-8648000102c1865d

Treiman, A. H. (2007). Geochemistry of Venus' Surface: Current limitations as future opportunities. *Exploring Venus as a Terrestrial Planet*, 7–22. https://doi.org/10.1029/176gm03

Wirth, R. (2009). Focused Ion Beam (FIB) combined with SEM and TEM: Advanced analytical tools for studies of chemical composition, microstructure and crystal structure in geomaterials on a nanometre scale. *Chemical Geology*, *261*(3–4), 217–229. https://doi.org/10.1016/j.chemgeo.2008.05.019

Zolotov, M. Y. (2018). Gas–Solid Interactions on Venus and Other Solar System Bodies. *Reviews in Mineralogy and Geochemistry*, *84*(1), 351–392. https://doi.org/10.2138/rmg.2018.84.10

Appendix. Tables and Figures

Table 1. Venera and Vega geochemical analyses of Venus' surface rock compositions, in weight percent oxide with 2-sigma errors, adapted from Dyar et al. (2020).

Element (wt% oxide)	Venera-13[a]	Venera-14[a]	Vega-2[b]
SiO_2	45.1 ± 3.0	48.7 ± 3.6	45.6 ± 3.2
TiO_2	1.59 ± 0.45	1.25 ± 0.41	0.2 ± 0.1
Al_2O_3	15.8 ± 3.0	17.9 ± 2.6	16.0 ± 1.8
FeO	9.3 ± 2.2	8.8 ± 1.8	7.74 ± 1.1
MnO	0.2 ± 0.1	0.16 ± 0.08	0.14 ± 0.12
MgO	11.4 ± 6.2	8.1 ± 3.3	11.5 ± 3.7
CaO	7.1 ± 0.96	10.3 ± 1.2	7.5 ± 0.7
K_2O	4.0 ± 0.63	0.2 ± 0.07	0.1 ± 0.08
S	0.65 ± 0.4	0.35 ± 0.31	1.9 ± 0.6
Cl	<0.3	<0.4	0.3

[a]Barsukov et al. (1982).
[b]Barsukov et al. (1986).
Na_2O was not measured.

Table 2. Chemically active major and trace gases in Venus' atmosphere. Adapted from Fegley (2014) and Zolotov (2018).

Gas	Concentration	Altitude
CO_2	96.5 ± 0.8%	<65 km
N_2	3.5 ± 0.8%	<65 km
SO_2	150 ± 30 ppmv	22-42 km
H_2O	30 ± 15 ppmv	5-45 km
CO	17 ± 1.4 ppmv	12 km
COS	4.4 ± 1 ppmv	33 km
H_2S	3 ± 2 ppmv	<20 km
S_n	20 ppbv	<50 km
HCl	0.4 ± 0.03 ppmv	0-74 km
HF	5 ± 3 ppbv	35-70 km

Table 3. EPMA analyses of starting materials (Teffeteller et al., 2020, 2021a, 2021b).

Wt. % oxide	Synthetic tholeiitic basalt	Natural alkaline basalt
SiO_2	48.9	47.9
TiO_2	1.3	2.8
Al_2O_3	18.2	18.0
Cr_2O_3	0.5	0.0
FeO	10.1	9.6
MnO	0.2	0.1
MgO	8.3	3.3
CaO	10.2	7.7
Na_2O	2.1	6.0
K_2O	0.2	2.7

Table 4. Experimental runs with sample compositions, conditions, and durations.

Sample	Composition	Run Conditions	Duration
VS-1A	alkaline	700°C, 90 bars	14 days
VS-1B	tholeiite	700°C, 90 bars	14 days
VS-3A	alkaline	470°C, 90 bars	22 days
VS-3B	tholeiite	470°C, 90 bars	22 days
VS-4A	alkaline	470°C, 90 bars	30 days
VS-4B	tholeiite	470°C, 90 bars	30 days

*All runs conducted with a magnetite-hematite + pyrite buffer assemblage.

Table 5. Alteration product coverage of reacted alkali and tholeiite samples.

Run	Temperature	Duration	Alkali (%)	Tholeiite (%)
VS-1	700°C	15 days	70	27
VS-3	470°C	22 days	40	0.4
VS-4	470°C	30 days	20	0.2

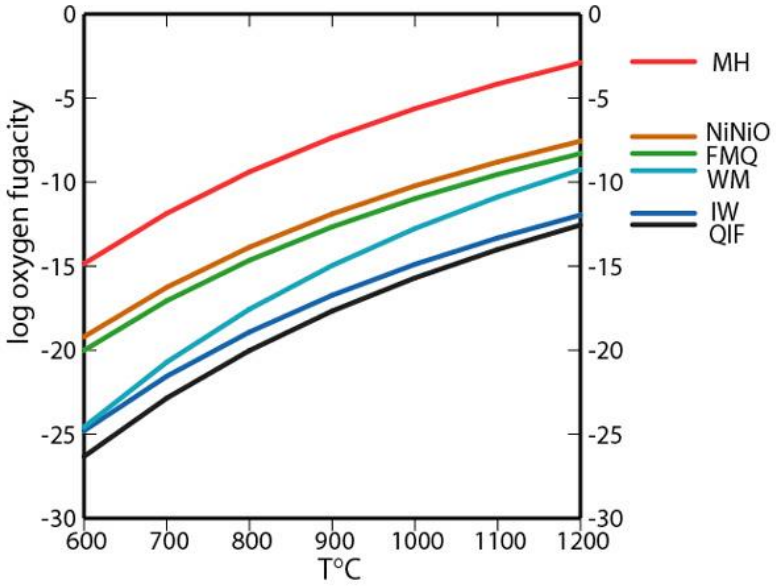

Figure 1. Log oxygen fugacity (fO_2) of several mineral redox buffers plotted as a function of temperature at 1 bar pressure. Venus' surface fO_2 is estimated to near the magnetite-hematite (MH) buffer curve. Redox curves were plotted using data from Frost (1991) and published at https://en.wikipedia.org/wiki/Mineral_redox_buffer.

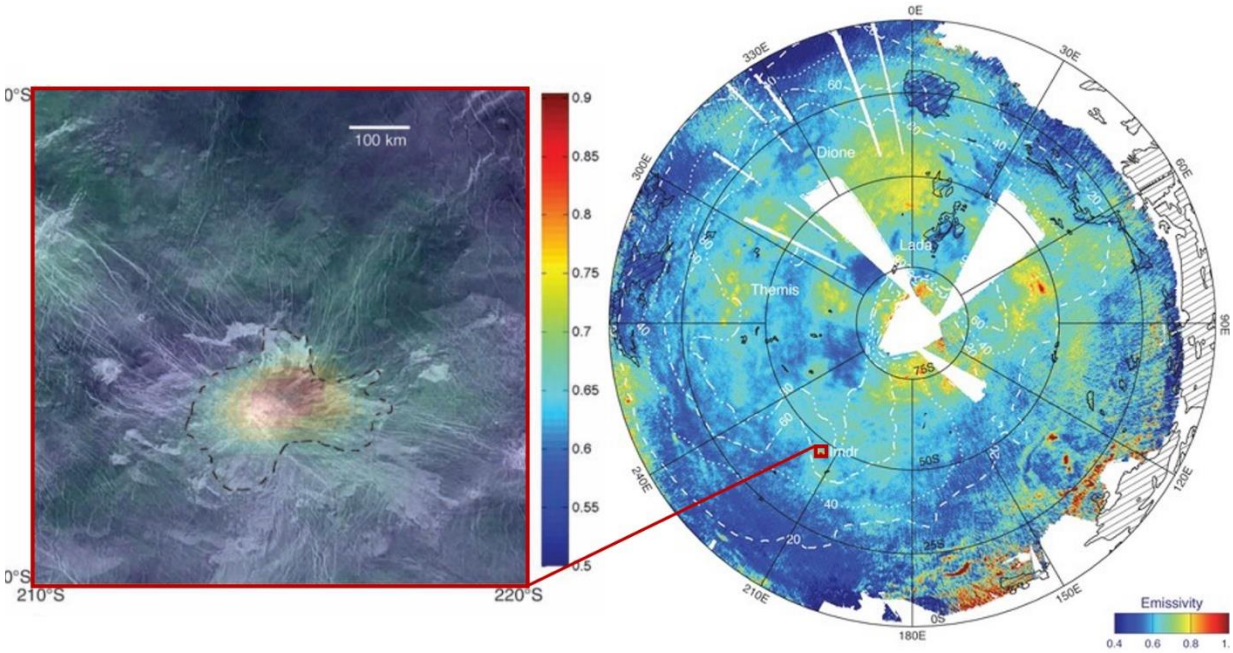

Figure 2. VIRTIS Emissivity data with superimposed Magellan SAR map of the volcano Idunn Mons (*L*) and emissivity in Venus' southern hemisphere (*R*). The small red box shows the location of Idunn Mons within hotspot Imdr Regio. Emissivity values are represented in the color-coded scale bars. Modified from Smrekar et al. (2014).

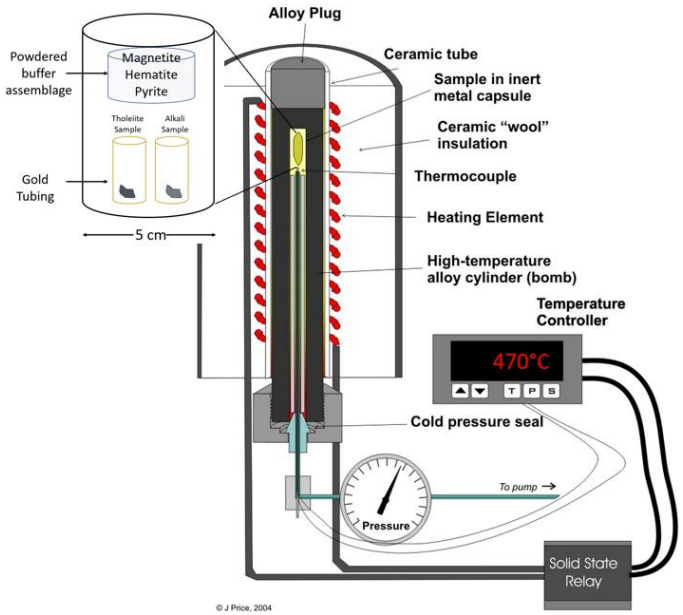

Figure 3. Schematic of a generic cold-seal pressure vessel apparatus. The inset illustrates the size and layout of the sample chamber (modified from Price, 2004).

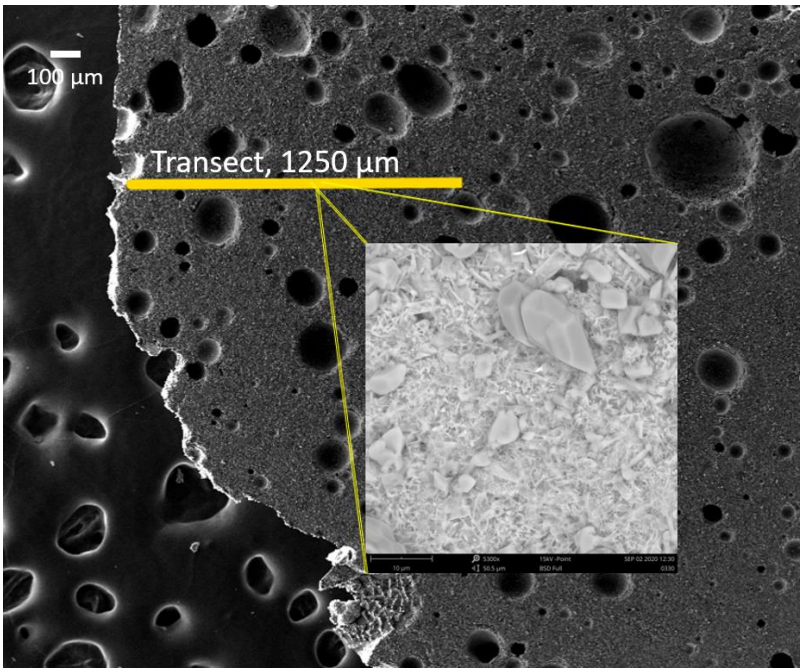

Figure 4. A representative transect superimposed on a SEM microphotograph of the surface of a basalt sample. The inset depicts 1 of 25 backscatter electron images of the surface that comprise the transect. Each BSE image has a field of view of ~50 µm.

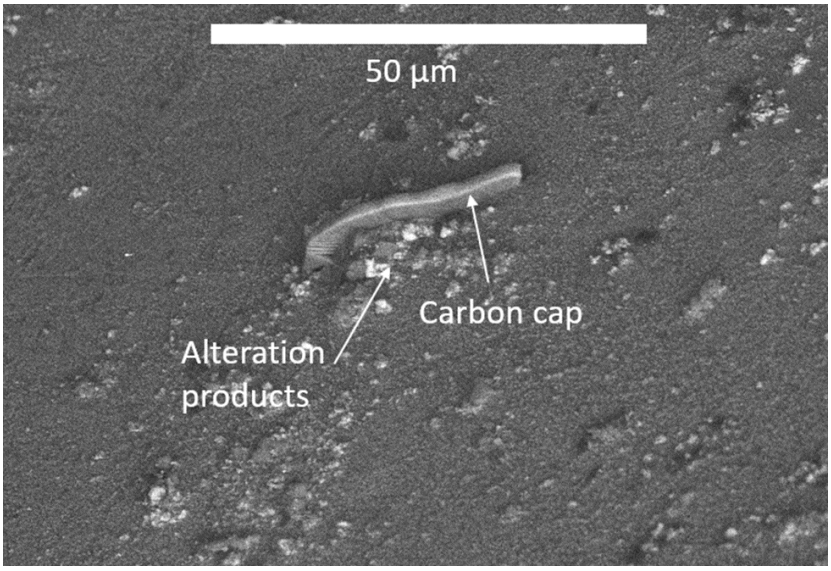

Figure 5. SEM z-contrast photomicrograph of a FIB milling protective carbon cap. The cap is seen on the surface of the tholeiitic sample VS-1B (700°C).

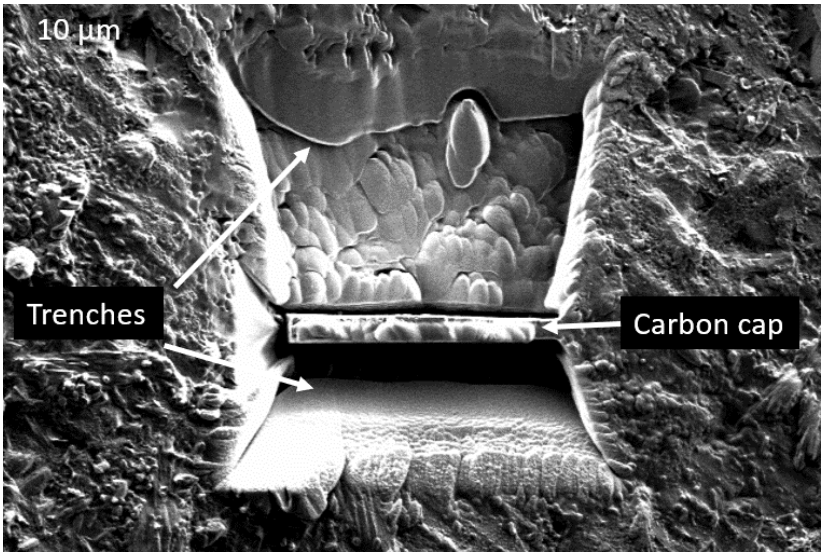

Figure 6. SEM secondary electron microphotograph of the surface of a sample after gallium ion milling of two opposing trenches that defined the FIB cross-section.

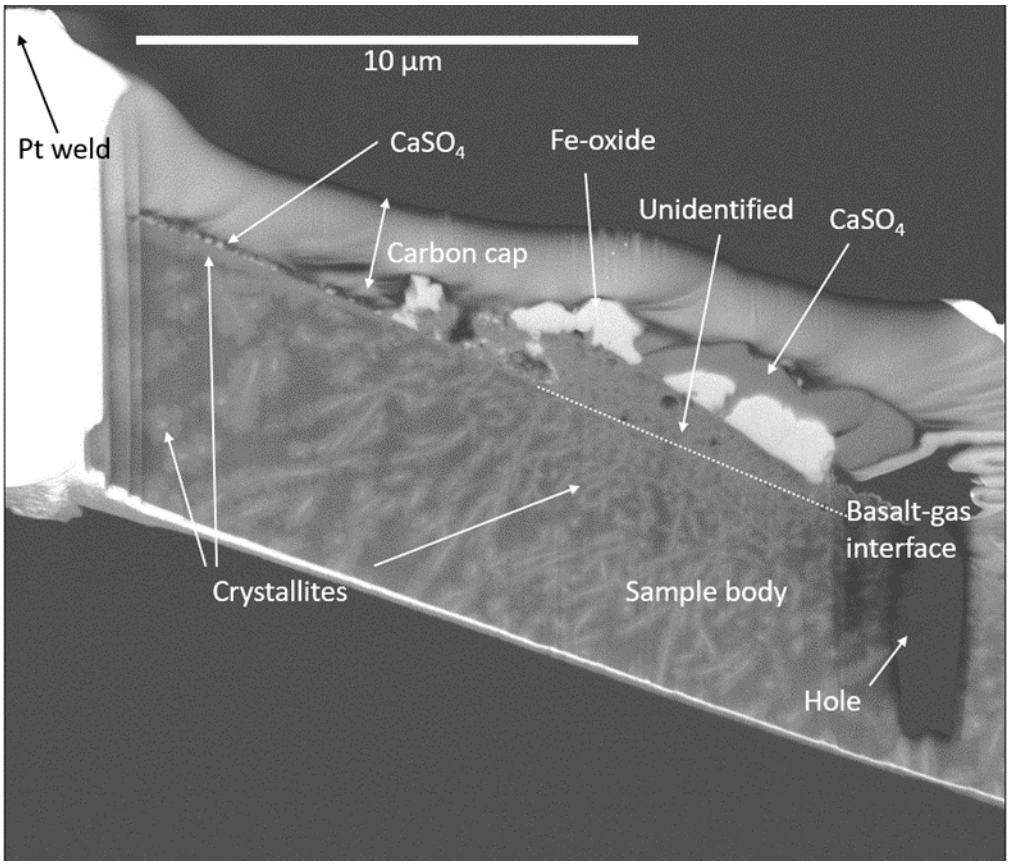

Figure 7. SEM z-contrast microphotograph of completed FIB cross-section from specimen VS-1B. The persistence of the carbon cap shielded the surface reaction products and subsurface from ion bombardment. This specimen was polished to approximately 80–100 nm thick.

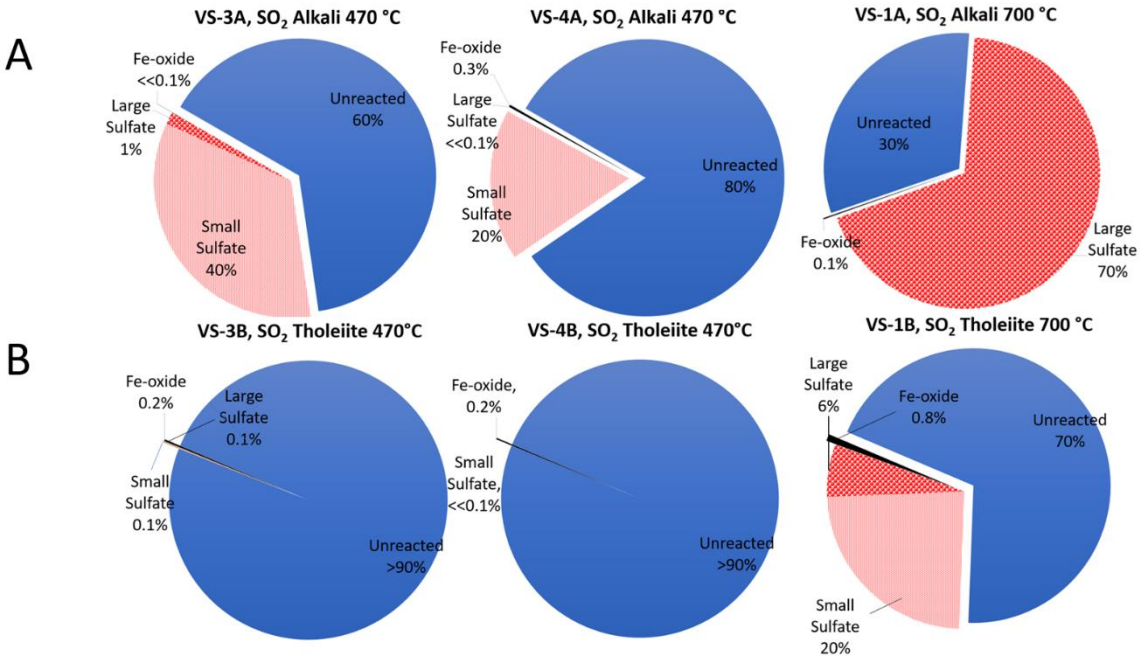

Figure 8. Graphic depicting alteration product relative abundances on alkali (A) and tholeiite (B) specimens. Left to right, 470°C runs were conducted for 3- and 4-week durations, respectively, and the 700°C run was 2 weeks. Sulfate products appearing on the alkali samples were metathenardite and anhydrite on tholeiite samples. Large sulfates were ≥1 μm and small sulfates were <1 μm.

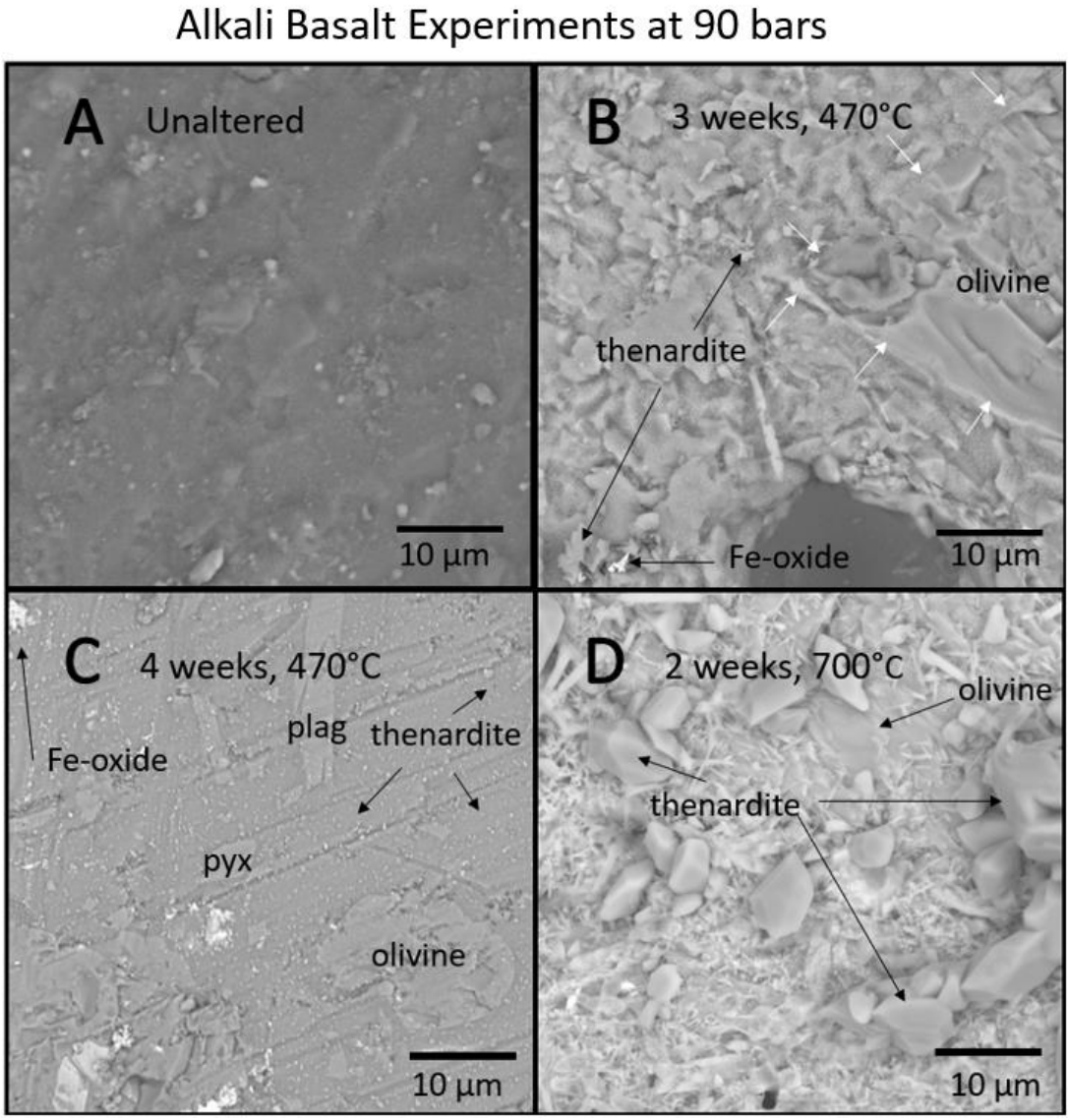

Figure 9. SEM BSE images of alkali samples. A) Unaltered; B) Alteration for 3 weeks at 470°C, 90 bars, showing thenardite and Fe-oxide alteration phases and olivine grain boundary (white arrows); C) 4 weeks at 470°C, 90 bars, showing nanoscale thenardite and Fe-oxide alteration products and microphenocrysts of plagioclase (plag), pyroxene (pyx), and olivine. Parallel lines are from sample preparation; D) 2 weeks at 700°C, 90 bars, exhibiting euhedral thenardite crystals up to several microns in size and a relatively bare surface of an olivine grain.

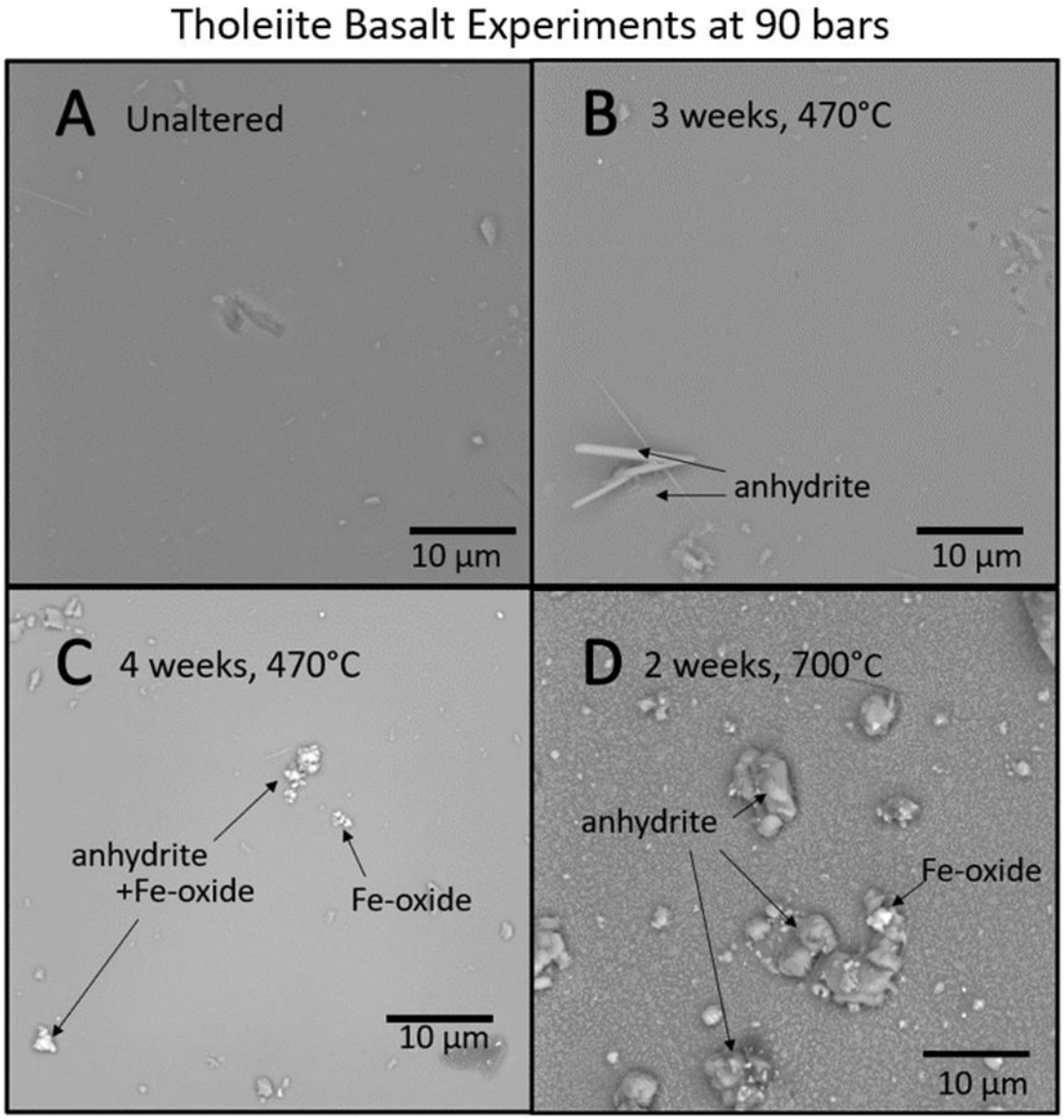

Figure 10. SEM BSE images of tholeiite samples. A) Unaltered; B) Alteration for 3 weeks at 470°C, 90 bars, showing a prevalent vitreous surface with nanophase- and ~10 µm acicular anhydrite and Fe-oxide alteration phases; C) 4 weeks at 470°C, 90 bars, showing nanoscale anhydrite and Fe-oxide alteration products in heterophase masses and discrete Fe-oxide grains on a glassy surface; D) 2 weeks at 700°C, 90 bars, exhibiting a nearly continuous and evenly distributed dusting of nano-scale anhydrite grains with cluster of subhedral thenardite crystals up to several microns in size in heterophase masses with minor Fe-oxides.

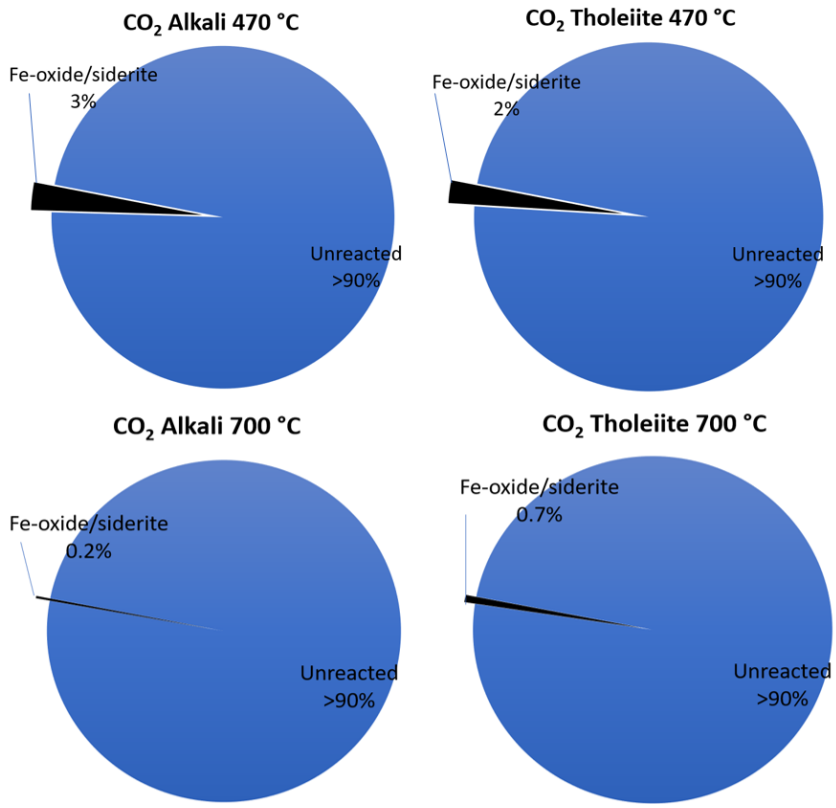

Figure 11. Graphic showing estimated abundances of alteration phases on run products reacted in pure CO_2. Alkali (left) and tholeiite (right) samples were reacted for 2-weeks at 470°C and 700°C in pure CO_2 under 90 bars pressure.

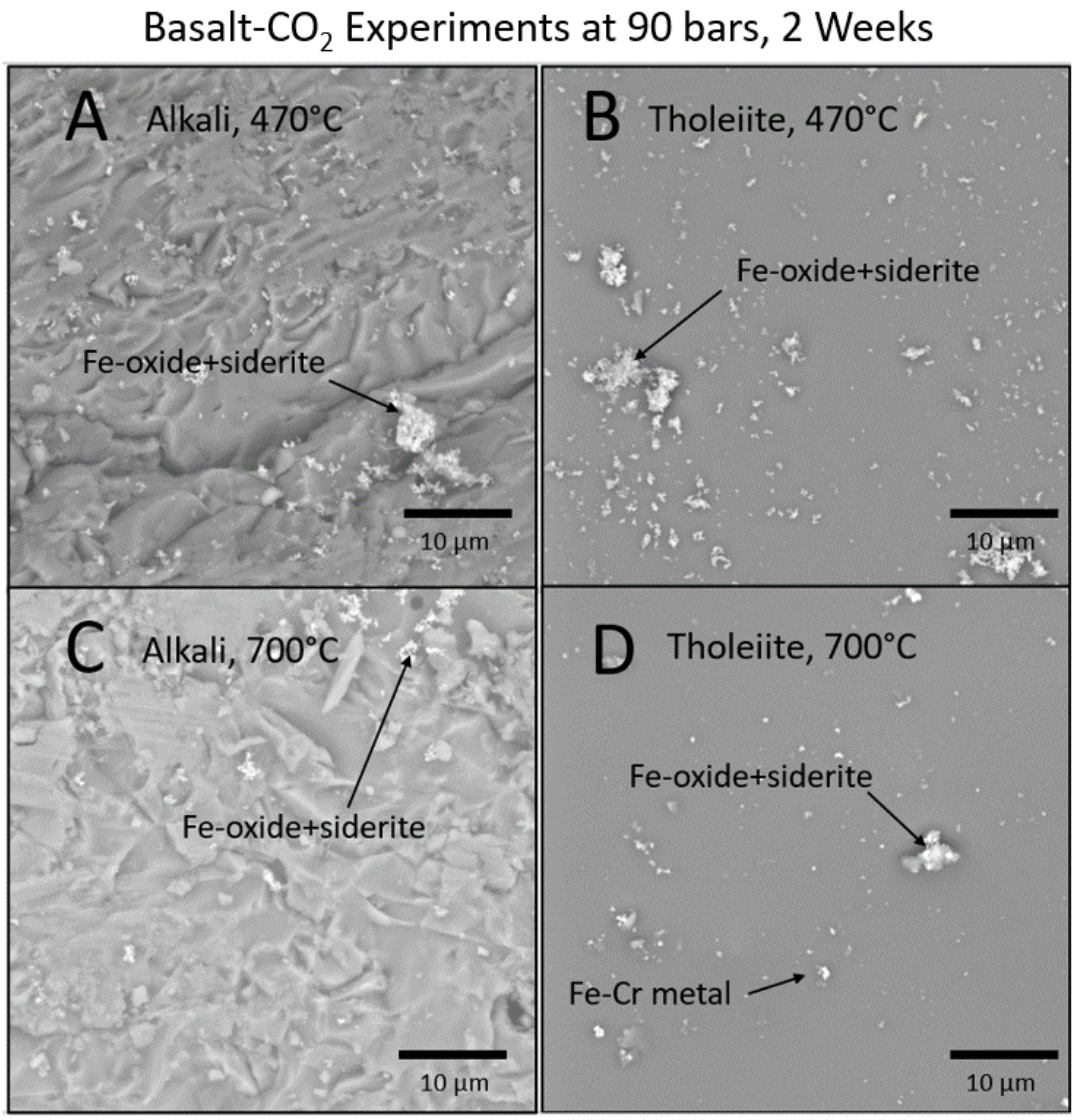

Figure 12. SEM BSE microphotographs of samples reacted for two weeks in pure CO_2 at 90 bars. A) Alkali 470°C; B) Tholeiite 470°C; C) Alkali 700°C; D) Tholeiite 700°C. On each sample, Fe-oxide and siderite ($FeCO_3$) phases are present together in clusters of <1 µm grains, which makes them indistinct from one another.

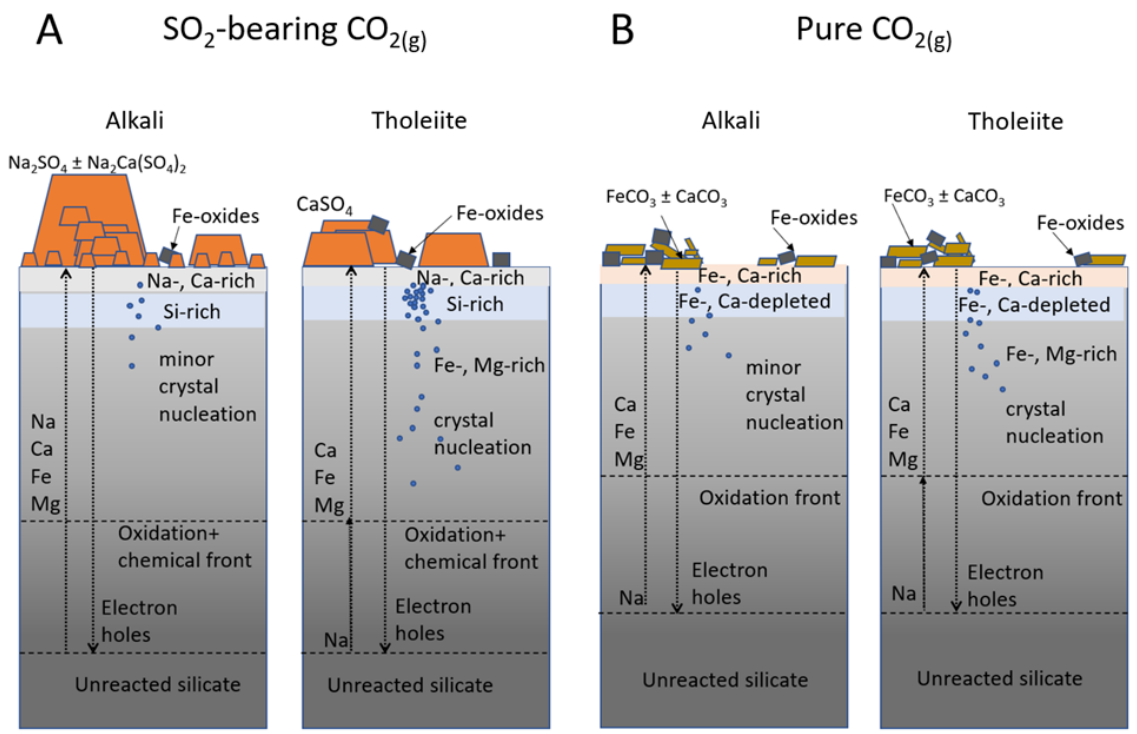

Figure 13. Schematic depicting basalt glass reactions in gases at 470°C, 90 bars pressure for 2 weeks at MH fO_2. **A)** Alkali and tholeiite basalts react with an SO_2-bearing atmosphere that exerts both an oxidation potential gradient and a reaction driving force, creating reaction fronts in the solids. Surface Na and Ca react immediately with adsorbed SO_2. Na, Ca, Fe, and Mg cations diffuse through the glass toward the free surface in response to the redox and chemical gradients. Cation diffusion is countered by an inward flux of electron holes that oxidize Fe^{2+} to Fe^{3+} in the subsurface, where Fe^{3+} is charge compensated by Na. If the concentration of Na is sufficient to stabilize Fe^{3+} (i.e., the alkaline composition), then Na outpaces other diffusing cations to the surface where it enriches the near surface region and then reacts with SO_2 at the surface-atmosphere interface to form Na_2SO_4. In the tholeiite composition, the concentration of Na is inadequate to stabilize all of the oxidizing Fe in the subsurface, which nucleates as Na-rich pyroxenes and Fe-oxide spherulites. Near-surface Fe is oxidized to form magnetite ± hematite, while near-surface Ca reacts with atmospheric SO_2 to form anhydrite (Modified from Renggli and King, 2018 and interpreted from Cook et al., 1990; Cooper et al., 1996; Renggli et al., 2019). **B)** In a pure CO_2 atmosphere (interpreted from data from Teffeteller et al., 2020, 2021b), reaction phenomena are similar; however, the chemical driver of diffusive cation migration is solely an oxidation potential. The role of Na in the glass is maintained; however, it is either not reacted at the surface, or phase(s) are amorphous or too small to be observed. Other network modifying cations, Ca, Fe, and Mg, migrate toward and enrich a zone near the surface. Just beneath this layer, the glass is depleted in Ca, Fe, and Mg. At the surface, Fe^{2+} partially oxidizes to Fe^{3+} and reacts with CO_2 to form magnetite ($3FeO + CO_2 \rightarrow Fe_3O_4 + CO$; Zolotov, 2018), which reacts further with CO_2 to produce siderite ($Fe_3O_4 + 3CO_2 \rightarrow FeCO_3 + ½\ O_2$) or is again oxidized to form hematite ($Fe_3O_4 + CO_2 \rightarrow FeCO_3 + Fe_2O_3$) (Koziol, 2004). Additionally, Ca at the surface and migrating from the interior reacts with atmospheric CO_2 to form nano-scale or amorphous $CaCO_3$ (calcite) (Dyar et al., 2020) that may coexist with nano-scale or amorphous siderite.

Vita

Robert Reid received his Bachelor of Science degree with Honors in geology in 2019 from the University of West Georgia. There, he conducted research on tectonic and petrologic problems in the Southern Appalachians and in the Brevard Zone in western Georgia, which was presented at National and Southeast Regional GSA conferences, and he was the recipient of several departmental awards, including the James Emory Boyd Award, honoring the top geology student of 2019. He also obtained a Fundamentals of Geology certificate (GIT) from the National Association of State Boards of Geology. Thereafter, he pursued a Master of Science degree in geology at the University of Tennessee, Knoxville, Department of Earth and Planetary Sciences, under advisor Dr. Molly McCanta, where he studied chemical alteration of basaltic rocks on the surface of Venus. He was awarded the department's GEOL 596 Colloquium Presentation Award and conducted research with colleagues from the Lunar and Planetary Science Institute and NASA's Johnson Space Center Astromaterials Research and Exploration Science Division. He presented the group's work at the Lunar and Planetary Science Conference and to the East Tennessee Geological Society.